AEDC-TR-72-14

cy 2

AN ANALYTICAL INVESTIGATION OF THE CASELESS ROCKET MOTOR

C. E. Willbanks, R. C. Bauer, and P. T. Harsha

ARO, Inc.

February 1972

Approved for public release; distribution unlimited.

ENGINE TEST FACILITY
ARNOLD ENGINEERING DEVELOPMENT CENTER
AIR FORCE SYSTEMS COMMAND
ARNOLD AIR FORCE STATION, TENNESSEE

NOTICES

When U. S. Government drawings specifications, or other data are used for any purpose other than a definitely related Government procurement operation, the Government thereby incurs no responsibility nor any obligation whatsoever, and the fact that the Government may have formulated, furnished, or in any way supplied the said drawings, specifications, or other data, is not to be regarded by implication or otherwise, or in any manner licensing the holder or any other person or corporation, or conveying any rights or permission to manufacture, use, or sell any patented invention that may in any way be related thereto.

Qualified users may obtain copies of this report from the Defense Documentation Center.

References to named commercial products in this report are not to be considered in any sense as an endorsement of the product by the United States Air Force or the Government.

AN ANALYTICAL INVESTIGATION OF THE CASELESS ROCKET MOTOR

C. E. Willbanks, R. C. Bauer, and P. T. Harsha
ARO, Inc.

FOREWORD

The work reported herein was sponsored by the Air Force Rocket Propulsion Laboratory (AFRPL) under Program Element 61101F, Project 3059. The AFRPL project monitor was Timmy C. Aden, First Lieutenant, USAF.

The results of the research presented were obtained by ARO, Inc. (a subsidiary of Sverdrup & Parcel and Associates, Inc.), contract operator of the Arnold Engineering Development Center (AEDC), Air Force Systems Command (AFSC), Arnold Air Force Station, Tennessee, under Contract F40600-72-C-0003. The investigation was conducted in the Engine Test Facility (ETF) under ARO Project No. RW5174 from June 1970 to June 1971, and the manuscript was submitted for publication on October 14, 1971.

This technical report has been reviewed and is approved.

Eules L. Hively
Research and Development
Division
Directorate of Technology

R. O. Dietz
Acting Director
Directorate of Technology

ABSTRACT

An analysis of a caseless and nozzleless solid-propellant rocket motor employing the external burning concept was made. Performance was calculated for a wide range of supersonic flight conditions. The results of the analysis show that acceptable values of specific impulse and thrust are possible for propellants having sufficiently high burn rates in a base burning configuration. The effect of boattailing with combustion along the boattail was investigated and found to degrade the performance. An analysis of a thin planar airfoil with external burning occurring on part of its surface was also made. The specific lift, that is the ratio of the lifting force to propellant flow rate, was found to be an order of magnitude lower than the corresponding specific lift for a conventional airfoil propelled by a turbine engine.

CONTENTS

		Page
	ABSTRACT	iii
	NOMENCLATURE	vi
I.	INTRODUCTION	1
II.	ANALYSIS	
	2.1 Pure End Burning Configuration	2
	2.2 Performance of a Boattail Configuration	6
	2.3 Phenomenology of Propellant Combustion	8
	2.4 External Burning on a Thin Planar Airfoil	9
III.	CONCLUSIONS	13
	REFERENCES	14

APPENDIX
ILLUSTRATIONS

Figure

1. Configuration of the Caseless Rocket Motor
   a. Pure End Burning . . . 19
   b. Boattail . . . 19
2. Base Pressure Ratio versus Dimensionless Burn Rate . . . 20
3. Boundary Layer Separation Criterion of Arens and Spiegler . . . 21
4. Schematic of Interaction of External Flow and Propellant Gases . . . 22
5. Maximum Base Pressure . . . 23
6. Forebody Drag Coefficient versus Maximum Cruise Mach Number . . . 24
7. Maximum Net Thrust Parameter versus Flight Mach Number . . . 25
8. Net Thrust versus Burn Rate . . . 26
9. Range versus Time . . . 27
10. Schematic of Caseless Rocket Motor with Boattail . . . 28
11. Boattail Pressure versus Mass Addition Rate along the Boattail . . . 29
12. Specific Impulse of Mass Flow Injected along Boattail versus Boattail Mass Addition Rate . . . 30
13. Schematic of Deflagration in a Solid Propellant . . . 31
14. External Burning Applied to Thin Planar Airfoil for Propulsion or Lift . . . 32
15. Comparison of Theory with Experimental Data of Fernandez and Zukoski . . . 33
16. Pressure Ratio versus Mass Injection Parameter . . . 34
17. Specific Thrust for $\theta = \theta_{max}$ . . . 35
18. Normal Force Coefficient as Compiled in Ref. 1 . . . 36
19. Specific Lift for Thin Planar Airfoil . . . 37

NOMENCLATURE

A_b	Base Area
A_s	Secondary flow area at choke point
C	Crocco number
C_D	Drag coefficient
C_{n_f}	Normal force coefficient
C_p	Specific heat
h	Airfoil thickness
I_n	Integral formula (Eq. (14))
I_{sp}	Specific impulse
L_g	Gross lift
L_{sp}	Specific lift
ℓ	Airfoil length
M	Mach number
m_o	Initial mass of vehicle
$\dot{m}$	Mass flow rate
P	Static pressure
R	Body radius
$\bar{R}$	Universal gas constant
R_p	Plume radius of curvature
r	Burn rate
S	Distance
T	Static temperature
T_g	Gross thrust

T_n	Net thrust
T_o	Total temperature
T_{sp}	Specific thrust
t	Time
U	Velocity component in X direction
V	Velocity component in Y direction
W	Molecular weight
X	Axial coordinate
Y	Normal coordinate
α	Flow deflection angle
β	External flow angle
γ	Ratio of specific heats
η	Similarity variable = $\sigma Y/X$
θ	Boattail angle
ν	Initial plume angle
ρ	Density
σ	Mixing zone spreading parameter
ϕ	Velocity ratio in mixing zone
ψ	Angle of equivalent inviscid flow

SUBSCRIPTS

A	External flow after deflection
b	Base
c	Boattail on lower edge of mixing zone
cr	Cruise

D	Dividing streamline
m	Extremeties of the mixing zone
w	Surface of planar airfoil
l	External flow
∞	Free stream

SECTION I
INTRODUCTION

Currently, all aircraft and rocket propulsion systems using chemical propellants employ internal combustion. That is, combustion occurs in a chamber at high pressure relative to ambient pressure, and the resulting high temperature gas is expelled through a nozzle or turbine to generate thrust for propulsion. At supersonic flight speeds, relatively small deflections of the external flow over a body can result in a significant alteration of the pressure distribution or a body. Hence, burning a propellant externally, either in the flow field adjacent to a body or near the surface of the body, permits some degree of control over the pressure distribution. External burning for attitude control, drag reduction, and propulsion has been studied for a number of years. Billig (Ref. 1) reviews the unclassified studies on external burning prior to 1967.

Several studies have been concerned with the thrust increment available if a propellant is injected from the side of an aerodynamic body into the adjacent external flow. The propellant may be balanced or fuel-rich or may simply be a fuel which depends on mixing with air for combustion. The magnitude of the thrust increment is highly dependent on the location of the combustion zone in the flow field relative to the body; thus the nature of propellant injection and the rates of mixing and chemical reaction are important considerations in determining performance. This scheme has been investigated both experimentally and analytically. Of the recent unclassified literature, the work of Strahle (Ref. 2) on this scheme is probably most notable.

Considerable effort has been devoted to drag reduction through injection of a propellant or fuel into the base region of a body. If combustion occurs in the near wake region, an increase in base pressure is experienced. Among the studies of this problem are those of Davis (Ref. 3) and Koh (Ref. 4).

Another approach involves the use of an ablative material as the propellant. The forebody of the vehicle is composed of a combustible material which ablates and is carried into the base region by mixing where it burns with an attendant increase in base pressure. Injection is eliminated in this scheme.

The configurations considered in the present study are somewhat different in concept from those previously investigated in that a caseless solid propellant is used. Elimination of the case simplifies the construction of the device, while at the same time improving the range available for a given specific impulse and given propulsion system volume. Two projectile configurations are considered. The simpler of the two is a pure end-burning configuration as shown in Fig. 1a; this may be considered the "baseline" configuration. In it, the propellant gases are considered to leave the burning region at sonic velocity, and the maximum pressure available at the base is governed by the pressure required to separate the turbulent boundary layer on the sides of the body. The "boattail" design shown in Fig. 1b was also investigated. In this configuration, burning is assumed to occur along the sides as well as on the base of the projectile. The Mach number range of interest is from 2 to 6.

It might be noted that the concept of the end burning configuration is in many ways similar to the "traveling charge" concept used in interior ballistics of guns (Ref. 5).

An analysis to determine the lift and thrust of a thin planar airfoil with burning at its surface is also presented. Surface burn rates are limited to values permitting complete entrainment of the propellant gases into the external flow by the turbulent mixing zone.

In the following sections, the analytical approaches chosen and the results obtained are described in detail.

SECTION II
ANALYSIS

2.1 Pure End Burning Configuration

The pure end burning caseless rocket motor (CRM) shown schematically in Fig. 1 will be analyzed first. Only an approximate analysis based on several simplifying assumptions is possible in view of the lack of understanding of the combustion process itself. The flight Mach number range of interest is from 2 to 6.

It is well known that a small amount of mass addition to the base region of a bluff-base body in supersonic flight raises the base pressure by a large amount (see, for example, Ref. 6). Through large rates of mass addition, the base pressure can be made to approach the free-stream static pressure. At this point, an increase in the rate of mass addition ceases to affect the base pressure significantly. If the mass addition is uniformly distributed over the base (effectively a subsonic nozzle that occupies the entire base area), this trend of increasing base pressure continues until the velocity of the fluid added to the base becomes sonic at the base pressure. It is expected that further increase in the mass addition rate will raise the base pressure above the free-stream static pressure while the Mach number of the fluid entering the base remains sonic. The latter condition is equivalent to an underexpanded sonic nozzle occupying the entire base region. Similar behavior can be expected when the mass added to the base originates from the combustion of a propellant. The pressure at the end of the heat release zone at the propellant surface would be expected to have the variation with burn rate shown schematically in Fig. 2. To avoid restricting the analysis to particular propellants, it will be assumed that a propellant can be formulated to yield the required burn rate at a given base pressure.

The thrust developed at the burning surface is made up of two components. One component is the static pressure. The second component is the momentum flux of the gases leaving the surface. To achieve maximum thrust for propulsion of a vehicle at zero angle of attack, it appears that the burning surface should be planar and normal to the direction of motion.

If the gas-phase reaction zone is thin compared with the base diameter, a pressure gradient normal to the propellant interface must exist in the heat release portion. The

situation is similar to Rayleigh-type flow, heating in a constant area tube. Since the flow must be subsonic, the pressure at the beginning of the heat release zone must be larger than the pressure at the end of the heat release zone. The pressure over any cross section parallel to the propellant surface in the heat release zone is assumed to be uniform. A discussion of the propellant combustion process follows in a later section.

In order to analyze the pure end burning rocket motor, the following assumptions are made:

1. The gas-phase reacting zone is thin.
2. The products of combustion are perfect gases with constant specific heats.
3. The velocity of the condensed phase is small compared with the velocity of propellant gases after burning, both velocities being measured relative to the interface.
4. The flow is one dimensional and steady.

A momentum balance across the gas-phase reaction zone yields the following equation for gross thrust:

$$T_g = A_b P_b (1 + \gamma_b M_b^2) \tag{1}$$

The variable T_g is the total force exerted on the base of the propellant grain. Since thrust rather than drag reduction is the objective of the propulsion system under study, it will be assumed that the propellant gases leave the gas-phase reaction zone and enter the base at the sonic velocity. Further discussion of this assumption follows in a later section.

For $M_b = 1.0$, the thrust becomes

$$T_g = (1 + \gamma_b) P_b A_b \tag{2}$$

and clearly is determined by P_b. Although the maximum value which P_b may assume is subject to uncertainty, it is assumed that it is below the value which would cause the flow to separate from the body of the vehicle. For this study, it will be assumed that this is the mechanism governing the maximum base pressure. That is, the maximum value of P_b is the pressure for incipient separation of the flow over the vehicle. Moreover, P_b is determined from existing boundary layer separation criteria for two-dimensional fully developed turbulent boundary layers. The criterion of Ref. 7 was selected for this investigation, and separation pressure ratio versus Mach number is shown in Fig. 3.

The interaction of the external flow with the propellant gas flow is shown schematically in Fig. 4. The external flow is deflected through an angle (α) by the oblique shock, and the propellant gas must undergo a Prandtl-Meyer expansion in order to match the flow direction and pressure of the deflected external flow. The sharp corner can be maintained with the aid of a combustion inhibitor on the sides of the propellant grain.

Since the propellant gas is assumed to leave the flame zone at the sonic velocity, the maximum pressure ratio (P_b/P_1) can be determined as a function of the external flow Mach number (M_1) and the initial flow angle (β) for a given separation criterion. Figure 5 shows $(P_b/P_1)_{max}$ as a function of M_1 and β for $\gamma_b = 1.25$.

Equation (2) can be rearranged to give

$$T_g = (1 + \gamma_b)A_b\left(\frac{P_b}{P_1}\right)\left(\frac{P_1}{P_\infty}\right)P_\infty \tag{3}$$

It is evident from this equation that the maximum thrust level depends on vehicle geometry, flight Mach number, and flight altitude. From conservation of mass flow, the corresponding propellant mass flow rate necessary to maintain the thrust given by Eq. (3) is

$$\dot{m}_b = \frac{\gamma_b A_b\left(\frac{P_b}{P_1}\right)\left(\frac{P_1}{P_\infty}\right)P_\infty}{\sqrt{2\gamma_b \bar{R} T_{o_b}/(1 + \gamma_b)W_b}} \tag{4}$$

The specific impulse is

$$I_{sp} = \sqrt{2(1 + \gamma_b)\bar{A} T_{o_b}/\gamma_b W_b} \tag{5}$$

It can be noted that the specific impulse is identical to the specific impulse of a conventional rocket motor having a sonic nozzle. That is, the CRM has the same specific impulse as a sonic isentropic nozzle which occupies the entire base.

The net thrust for a vehicle propelled by a CRM is given by

$$T_n = A_b P_\infty \left[(1 + \gamma_b)P_b/P_\infty - \frac{\gamma_\infty C_D}{2} M_\infty^2 - 1\right] \tag{6}$$

where C_D is the forebody drag coefficient. This is the thrust available for acceleration.

Of particular interest is the case where $T_r = 0$, that is cruise conditions where thrust equals drag. The cruise Mach number is

$$M_{\infty_{cr}} = \sqrt{\frac{2(1 + \gamma_b)P_b/P_\infty - 2}{\gamma_\infty C_D}} \tag{7}$$

Figure 6 shows C_D as a function of maximum cruise Mach number with $(P_b/P_1)_{max}$ given by Fig. 5 and by assuming that the flow conditions at the aft end are essentially the same as the undisturbed flow conditions ahead of the vehicle, that is $P_A/P_1 = 1.0$. This would occur on a vehicle having a sharp nose and a long cylindrical afterbody. It should be noted that $M_{\infty_{cr}}$ is independent of altitude if C_D is independent of Reynolds number.

In order to illustrate the magnitude of thrust expected from a CRM and the accompanying specific impulse and propellant burn rate, a flame temperature (T_{o_b}) of 5000°R, a molecular weight of 25 lbm/lb mole, and a propellant density of 100 lbm/ft^3 (0.058 lbm/in.^{3}) are assumed. As evident from Eq. (5), the specific impulse is independent of altitude and flight Mach number, and equals 186 lbf sec/lbm for γ_b = 1.25.

Figure 7 shows the maximum net thrust parameter ($T_n/A_b P_\infty$) for the example above for a right circular cone and an ogive-cylinder as a function flight Mach number. The parameter is independent of altitude. Skin friction of the conical vehicle has been neglected, and the drag coefficient of the forebody of 0.1 corresponds to a 3.16 caliber von Kármán ogive-cylinder without skin friction. The maximum P_b/P_1 was determined from Fig. 5, and for the ogive-cylinder, the conditions at the aft end were taken to be the flight conditions of the vehicle.

Figure 8 shows the net vehicle thrust (T_n/A_b) as a function of propellant burn rate at sea level. The burn rate for cruise corresponds to T_n = 0.

Figure 9 gives the time required for an ogive-cylinder vehicle with C_D = 0.174 to travel a given distance from a launch Mach number of 1.5 for constant burn rate of 4.0 in./sec. Also shown in the figure is the vehicle flight Mach number at the time the target is intercepted. For example, if a vehicle has an initial mass of 4 lbm and a cross-sectional area of 2 in.^{2}, it takes 2.3 sec for the vehicle to travel 5000 ft. The corresponding intercept Mach number is 3.1.

From the results presented in Fig. 7, it is evident that relatively high maximum thrust levels can be sustained with the caseless rocket motor while attached flow over the vehicle is maintained. The maximum net thrust can be noted to increase with increasing cone half-angle, increasing flight Mach number, and decreasing altitude. As the cone angle increases, the forebody drag increases. However, a correspondingly higher base pressure is permitted since the propellant gases can expand through a greater angle at the corner, and the result is an increase in maximum net thrust. The results presented in Fig. 7 are based on the assumption of a fully developed turbulent boundary layer at the aft end of the body. This is a good assumption for the conical forebody at high Reynolds number. However, the separation ratio for the boundary layer on an ogive-cylinder may be lower than the fully developed value since the boundary layer develops in an adverse pressure gradient on the rear portion of the body. It should also be noted that maximum net thrust decreases with increasing altitude since the maximum thrust is proportional to atmospheric pressure. The maximum net thrust at sea level is about one hundred times greater than the value at 100,000 ft.

Figure 8 shows that the net vehicle thrust decreases as the cone angle is increased for a constant burn rate. This is a result of the increase in forebody drag associated with an increase in cone angle. The net thrust for all of the vehicles shown in Fig. 8 can be noted to decrease with increasing Mach number at a given burn rate. Figure 8 also shows that unusually high burn rates are required to sustain the thrust of a CRM. This can be attributed primarily to the small surface area for burning and secondarily to the somewhat lower specific impulse compared with a conventional solid-propellant rocket

motor. The burn rate is about one to two orders of magnitude higher than the burn rate in a typical solid-propellant combustion chamber. Moreover, this high burn rate must be accomplished at a pressure of one to two orders of magnitude lower than the combustion chamber pressure of a conventional solid-propellant rocket motor. For example, at sea level, the combustion pressure is on the order of four atmospheres. The combustion pressure decreases rapidly with increasing altitude.

2.2 PERFORMANCE OF A BOATTAIL CONFIGURATION

Aerodynamic bodies with boattails are known to generally have lower drag than corresponding bodies with cylindrical aft ends (Ref. 8). For example, boattail configurations are frequently found on turbojet engines, projectiles, and rocket-powered missiles. It is, therefore, of interest to study the caseless rocket motor with a boattail. The configuration is shown schematically in Fig. 1b. Combustion occurs on the boattail surface as well as on the circular base. As before, the propellant gases are assumed to leave the base portion at the sonic velocity.

Considerable work has been devoted to the study of boattail configurations and bluff base bodies with base bleed including the effects of combustion (Refs. 3 and 4). The behavior of the boattail configuration shown in Fig. 10 is similar to the case of massive blowing along the boattail itself. The mass added in the boattail region comes from burning at the boattail surface. No satisfactory analysis of this problem was found in the literature. Cole and Aroesty (Ref. 9) solved the inverse problem of massive blowing along a surface. In principle, the Cole and Aroesty approach should permit performance calculation for boattail configurations as well as more complex configurations such as waisted bodies, that is, "Coke® bottle" shapes. If the pressure distribution along the boattail is specified, its analysis can be used to calculate the corresponding mass injection distribution. In the present problem, the mass injection distribution along the boattail is known, and the corresponding pressure distribution is to be determined. It was found that numerical methods must be used to solve the direct problem and the Cole and Aroesty analysis was abandoned in favor of a more simplified approach. For purposes of analysis, the following assumptions are made:

1. The flow is inviscid and adiabatic.

2. The effect of burning along the boattail is simply to add hot gas between the external flow and the primary jet.

3. The shape of the primary jet plume is governed by the boattail pressure.

4. The pressure along the boattail is uniform.

5. The external flow is deflected through an oblique shock so that the pressure in the external flow matches the boattail pressure.

6. The trajectory of the streamline dividing the external flow from the flow originating along the boattail (secondary flow) is initially straight at the initial flow deflection angle and turns back parallel to the axis at the end of the boattail.

7. The secondary flow expands one dimensionally to the free-stream pressure and chokes at the minimum flow area between the external flow and primary jet plume.

8. The axial component of the momentum of the secondary flow is negligibly small because of the small angle of the boattail.

Clearly the restrictions imposed on the analysis by the assumptions cast doubt on the quantitative validity of the analysis; however, the results should have the correct order of magnitude and correct trends. The assumptions are justified by the complexity of a more exact analysis.

The shape of the primary jet plume boundary was determined from the approximate method of Ref. 10, which assumes the plume boundary to be a circular arc. The primary jet behaves as an underexpanded sonic nozzle. The assumptions listed above reduce the problem to one of a geometrical nature. The minimum flow area must be determined as a function of the external flow dividing streamline trajectory and the primary jet plume boundary shape. By referring to Fig. 10, it is easily verified that

$$A_s = A_b \left\{ \left(\frac{Y_A}{R_b}\right)^2 - 2\left(\frac{Y_A}{R_b}\right)\left(\frac{X_A}{R_b}\right) \tan\alpha + \left(\frac{X_A}{R_b}\right)^2 \tan^2\alpha - \left[\left(\frac{R_P}{R_b}\right)(1 - \cos\nu) + 1\right]^2 \right\} \quad (8)$$

The rate of secondary mass flow is

$$\dot{m}_c = \sqrt{\frac{\gamma_c(\gamma_c + 1)W_c A_s P_\infty}{2\bar{R}T_{o_c}}} \quad (9)$$

Thus for given external flow conditions, boattail geometry, propellant characteristics, and primary jet mass flow rate, the boattail pressure can be determined as a function of the secondary mass flow rate or burn rate along the boattail.

Figure 11 shows numerical results for Mach numbers of 3 and 4 and two boattail angles. The calculations were made for $\gamma_c = \gamma_b = 1.25$ and $T_{o_b}/T_1 = T_{o_c}/T_1 = 8.0$ and the value of P_b/P_∞ corresponding to incipient boundary layer separation for the pure end burning configuration. It is evident that very large rates of mass addition along the boattail are required to maintain the boattail pressure above the free-stream value. The specific impulse for the boattail is shown in Fig. 12. It is seen to be much lower than the specific impulse of the primary jet or pure end burning configuration.

It is well to point out that mixing between the streams, that is viscous effects, tends to decrease the base pressure in general. Thus, the inclusion of viscous effects in the analysis would yield a lower specific impulse than predicted on the basis of the inviscid theory. For very small rates of mass injection along the boattail, the boattail pressure is known to be governed by viscous phenomena, and the present analysis would be completely invalid. This case is of little interest in the present study in view of the accompanying boattail

pressures. The inviscid theory becomes applicable when the secondary mass flow becomes much greater than the viscous entrainment rates for the external flow and primary jet plume.

2.3 PHENOMENOLOGY OF PROPELLANT COMBUSTION

Obviously the CRM will require an "exotic" propellant. The combustion phenomena of the simplest solid propellants are very complex, and a complete understanding of the various mechanisms involved in the combustion process does not exist. Propellant engineers can predict the specific impulse of a conventional solid-propellant rocket motor having a given propellant formulation with reasonable certainty from thermochemical calculations. The prediction of thrust from theory is much less reliable. Thrust depends on propellant burn rate which is a function of chamber pressure and initial temperature. Theories for predicting propellant burn rate are unsatisfactory for design purposes, and empirical burn rate data are necessary for estimating the thrust of a solid-propellant rocket motor. The formulation of propellants with desired characteristics is more of an art than a science.

While a realistic mathematical model cannot be posed for the CRM propellant, it is instructive to consider in a general and elementary way some of the individual mechanisms and processes associated with the overall combustion process.

Burning at the propellant interface may be viewed as the steady deflagration of a solid material. A simplified model of the process is shown in Fig. 13. In the condensed-phase reaction zone, complex phase transitions and chemical processes result in the evolution of gases which flow into the gas-phase reaction zone. The gases react exothermally in the gas phase and leave the zone as combustion products. This zone is similar to a premixed laminar flame. Combustion in the gas-phase reaction zone is similar to a stationary deflagration wave in a gas. Strong stationary deflagrations in gases are not observed to occur in practice. A strong deflagration is one in which the gases enter at subsonic speeds and leave at supersonic speeds relative to the wave. For the assumption of simple stagnation temperature change in planar flow, strong deflagration can easily be shown to violate the second law of thermodynamics (Ref. 11). If the flow is unsteady or locally non-one dimensional, this thermodynamic argument is not necessarily applicable. However, it appears that the assumption that the combustion products leave the reaction zone at the sonic velocity is not inconsistent with the laws of thermodynamics and may represent a limiting case for high burn rates.

By conservation of mass flow, the propellant burn rate is equal to the rate of gasification in the condensed-phase reaction zone. For most solid propellants, the gasification process is endothermic and the rate of gasification depends on the rate of heat added to the zone as well as the kinetics of the chemical reactions in the zone. Normally heat is added to the gasification zone by conduction and radiation from the hot gaseous reaction zone. If the rate of gasification is limited by heat transfer, an increase in the rate can be accomplished by adding ingredients to the propellant which react exothermally in the liquid or solid phase. The kinetics of the chemical reaction in the condensed-phase reaction zone are governed primarily by temperature, which itself depends on the rate of heat addition to the zone. Thus, a large rate of gasification can be obtained through large rates of heat release in the condensed-phase reaction zone.

For very large gasification rates, the limiting mechanism may become the gaseous-phase reaction rates. The kinetics of reaction in this zone must be sufficiently high to complete reaction in a thin flame zone. If the kinetics are not fast enough, the heat release will occur too far away from the base to raise the base pressure significantly and generate thrust. The kinetics of the gas-phase reaction zone depend principally on the temperature and composition of the gases entering the zone and the environmental pressure. The environmental pressure of the CRM cannot be controlled except within narrow limits. Thus the required reaction rate must be obtained with proper temperature and composition.

Unlike the conventional solid-propellant rocket motor, the heat loss by radiation from the burning surface of the CRM may represent a large fraction of propellant heat release. According to Williams (Ref. 12), the radiant heat loss generally depends on the fourth power of the surface temperature. The high surface temperature necessary for high gasification rates is accompanied by high radiation heat loss.

2.4 EXTERNAL BURNING ON A THIN PLANAR AIRFOIL

The end burning configuration of the CRM is primarily suited for application to rocket-powered projectiles. Figure 14 shows schematically the application of external burning to lift augmentation and propulsion of a thin planar airfoil. Either lift augmentation or thrust can be obtained depending on the airfoil geometry and angle of attack. The physics of the flow processes involved in this system are different from the physics of the end burning configuration.

In order to analyze the performance of this system, the following assumptions are made:

1. The pressure in Region II is uniform.
2. The rate of mass addition from burning along the aft surface is uniform.
3. All of the mass injected along the surface is entrained in the fully developed turbulent mixing layer between the surface and the external flow.
4. The fluids are perfect gases with constant specific heats.
5. The turbulent Prandtl, Schmidt, and Lewis numbers are unity.
6. There is no heat release in the mixing layer itself, that is, no afterburning.
7. The velocity, enthalpy, and concentration profiles are similar and are the same as for a planar turbulent free shear layer.

Assumption 3 limits the rate of mass addition to relatively small values.

The technique is essentially one of calculating the displacement thickness of the free shear layer. By referring to Fig. 14, it is easily verified that conservation of mass flow requires

$$(\rho V)_w = \frac{1}{\sigma}(\rho U)_A \cos(\theta + \alpha - \psi) \int_{\eta_w}^{\eta_D} \frac{\rho U}{\rho_A U_A} d\eta \tag{10}$$

where the mixing layer similarity variable ($\eta = \sigma Y/X$) has been introduced. After using the perfect gas equation of state and some basic fluid dynamic definitions, Eq. (10) becomes

$$\frac{(\rho V)_w}{(\rho U)_\infty} = \frac{1-C_\infty^2}{\sigma} \frac{C_A}{C_\infty} \frac{P_C}{P_\infty} \cos(\theta + \alpha - \psi) \int_{\eta_w}^{\eta_D} \frac{\phi}{\frac{W_A}{W}\left(\frac{T_o}{T_{oA}} - C_A^2 \frac{C_{P_A}}{C_P}\phi^2\right)} d\eta \tag{11}$$

where ϕ is the velocity U/U_A. Assumptions 1, 4, and 5 yield the result that reduced enthalpy and species concentration profiles are identical; thus Eq. (11) can be cast into the form

$$\frac{(\rho V)_w}{(\rho U)_\infty} = \frac{1-C_\infty^2}{\sigma} \frac{C_A}{C_\infty} \frac{P_C}{P_\infty} \cos(\theta + \alpha - \psi) \int_{\eta_w}^{\eta_D} \frac{\phi\left[\phi + (1-\phi)\frac{C_{P_w}}{C_{P_A}}\right] d\eta}{\left[\phi + (1-\phi)\frac{W_A}{W_w}\right]\left[\phi + (1-\phi)\frac{C_{P_w}}{C_{P_A}} - C_A^2\phi^2\right]} \tag{12}$$

Empirically it is known that the velocity profile in a free shear layer can be represented approximately by

$$\phi = \tfrac{1}{2}[1 + \mathrm{erf}(\eta)] \tag{13}$$

For convenience, the following integral relation is defined

$$I_n(\eta) = \int_{\eta_m}^{\eta} \frac{\phi^n\left[\phi + (1-\phi)\frac{C_{P_w}}{C_{P_A}}\right] d\eta}{\left[\phi + (1-\phi)\frac{W_A}{W_w}\right]\left[\phi + (1-\phi)\frac{C_{P_w}}{C_{P_A}}\frac{T_{o_w}}{T_{oA}} - C_A^2\phi^2\right]} \tag{14}$$

where n takes on values of 1 and 2. In order to compute this relationship, η_{-m} can be taken to equal -3.0. The trajectory of the equivalent inviscid boundary is defined by the relationship

$$\eta_A = \eta_m - (1 - C_A^2)(I_2)_{\eta_m} \tag{15}$$

which is based on the conservation of momentum. As with η_{-m}, the choice of η_m is not critical, and the value 3.0 is satisfactory. Conservation of mass flow requires

$$(I_1)_{\eta_D} = (I_1)_{\eta_m} - \frac{\eta_m - \eta_A}{1 - C_A^2} \tag{16}$$

This relationship implicitly determines the location of the dividing streamline.

Following Bauer (Ref. 13), the similarity parameter σ is determined by applying conservation of momentum and Prandtl's mixing length theory for the turbulent shear stress. The equation is:

$$\sigma = \frac{\pi \frac{W_A}{W_D}\left[\frac{T_{o_D}}{T_{o_A}} - C_A^2 \frac{C_{P_A}}{C_{P_D}} \phi_D^2\right](I_2)_{\eta_D} e^{2\eta_D^2}}{0.04235} \tag{17}$$

where $\sigma = 12$ for incompressible flow. The following geometric relations close the system of equations:

$$\tan \psi = \eta_A/\sigma \tag{18}$$

$$\tan (\theta + \alpha - \psi) = -\eta_w/\sigma \tag{19}$$

For a given free-stream condition, propellant characteristics, and afterbody angle (θ), Eqs. (12) through (19) can be solved simultaneously to yield the pressure ratio P_c/P_∞ as a function of the mass addition rate (burn rate) ratio $(\rho V)_w/(\rho U)_\infty$.

In order to gain some confidence in the method of analysis, a comparison with the experimental data of Fernandez and Zukoski (Ref. 14) was made. Fernandez and Zukoski studied supersonic flow over a flat plate with large distributed surface injection. The free-stream Mach number was 2.6, and both the primary stream and injected fluid were air with the same total temperatures. The deflection of the external flow as a function of the rate of surface injection was determined. As shown in Fig. 15, the theory compares favorably with the experimental data for mass injection ratios less than the blowoff value, that is, the maximum entrainment value. If the momentum flux of the injected fluid is neglected, the gross thrust is

$$T_g = h P_c \tag{20}$$

and the gross lift is

$$L_g = \ell P_c \tag{21}$$

The specific thrust referenced to the free-stream pressure is

$$T_{sp} = \frac{(P_c - P_\infty)\ell}{(\rho V)_w(\ell/\cos\theta)} \tag{22}$$

By using the tangent wedge approximation to relate the pressure change across the oblique shock (P_c/P_∞) to the flow deflection angle (a), it can be shown that the maximum thrust occurs when

$$\theta = (a + \theta)\left[\frac{1 - \frac{\gamma_\infty + 1}{2}(a + \theta)M_\infty}{2 - \frac{\gamma_\infty + 1}{2}(a + \theta)M_\infty}\right] \tag{23}$$

for a given rate of mass addition and a given afterbody length (ℓ). This value of θ is denoted by θ_{max}. For mass addition rates small enough to ensure complete mixing zone entrainment, the angle $(a + \theta)$ is only a weak function of θ itself, and θ_{max} is obtained by iteration. Although θ_{max} depends on M_∞ as well as other parameters, it is on the order of 4 deg. This small angle casts doubt on the practicality of the system for propulsion since useful levels of thrust or lift require extremely long airfoils.

Figure 16 shows P_c/P_∞ as a function of Mach number for hypothetical propellant characteristics. Although P_c/P_∞ is reasonably high, it can be noted to decrease rapidly with increasing θ and reaches unity when θ is approximately 8 deg. Large values of thrust can be obtained only at the expense of great airfoil length. Figure 17 shows the specific thrust for $\theta = \theta_{max}$. The specific thrust is obviously much lower than the value 1800 lbf-sec/lbm which typifies the fuel specific thrust of a turbojet engine.

In Fig. 18, the theoretical normal force parameter,

$$C_{n_f} = \frac{(P_c - P_c')\ell}{(\rho V)_w'\ell/\cos\theta} \tag{24}$$

and the normal force coefficient data are given from several external burning experiments and analyses as compiled and presented in Ref. 1. Here P_c' is the value of P_c for no mass addition or combustion. It is interesting to note that the value of C_{n_f} predicted by the present study agrees in magnitude with the experimental data of several studies. It should be pointed out that with a single exception, the experimental values or normal force coefficient are based on fuel flow alone. Thus, the experimental values based on fuel plus oxidizer would be lower.

Figure 19 illustrates the specific lift of an airfoil in the shape of a semi-diamond. The burn rate is the maximum for complete entrainment, and the pressure on the bottom of the airfoil is uniform since the wedge angle is made equal to $\theta_{max}/2$. The region of influence from the trailing edge interaction is assumed to be small. The wave drag is clearly zero. It is interesting to compare the specific lift

$$I'_{sp} = \frac{(P_c - P_\infty)2\ell}{(\rho V)_w \ell/\cos(\theta_m/2)} \tag{25}$$

with the specific lift of a typical turbojet-powered supersonic aircraft. For an aircraft with a lift-to-drag ratio of 8 and an engine specific thrust of 1800 lbf-sec/lbm, the specific lift is 14,400 lbf-sec/lbm, which is well above the value of 1000 for the airfoil of Fig. 18. Clearly such an airfoil could not compete with conventional turbojet-powered aircraft for normal transport operation. It should be pointed out that the aft end of the airfoil is consumed in flight since it is made of propellant. The accompanying problems of changing geometry and shifting centers of lift and mass must be considered in an application to a specific mission.

SECTION III
CONCLUSIONS

The analysis of the pure end burning caseless rocket motor (CRM) shows that acceptable specific impulse and high thrust levels are possible with solid propellants having sufficiently high burn rates. For typical propellant characteristics, the theoretical specific impulse was found to be 180 lbf-sec/lbm, which is somewhat lower than the specific impulse of a conventional solid-propellant rocket motor. However, for the same vehicle size and weight, more propellant can be utilized since the CRM operates without nozzle or combustion chamber hardware. Hence, for some missions, the range of a vehicle propelled by a CRM may be equal to the range of the same vehicle propelled by a conventional rocket motor. The maximum thrust calculations were made on the basis of maintaining attached flow over the vehicle forebody. The maximum thrust is reasonably high at low altitude and does not appear to present a serious limitation for many applications.

The performance of the CRM having a boattail was analyzed including the effect of burning along the boattail. The analysis showed that, in general, the boattail configuration has lower thrust and shorter range than the pure end burning CRM. It was found that large rates of mass addition from the combustion along the boattail are required to maintain the boattail pressure above the free-stream pressure even for small boattail angles. Moreover, the axial component of the momentum flux of the fluid leaving the boattail surface is very small except for large boattail angles. It should be pointed out, however, that the dynamic stability of the boattail configuration with burning may be better than the pure end burning configuration. Burning along the boattail creates an effective flare afterbody configuration. This aspect was not considered in the present study.

An analysis of a thin airfoil with external burning was also made. The analysis was restricted to burn rates sufficiently small so that complete entrainment of the combustion products in the mixing zone between the airfoil surface and the external flow occurred.

For these conditions, it was found that both thrust and lift could be obtained for the airfoil depending on the angle of attack. The theoretical normal force coefficient (lift) was found to agree in magnitude with data from several external burning experiments. However, from both a specific thrust and specific lift point of view, the performance of the airfoil was considerably below typical values for a turbojet-powered transport aircraft.

The CRM will require an "exotic" propellant. The required burn rate is one to two orders of magnitude higher than the burn rate in a conventional solid-propellant rocket motor. Moreover, combustion must occur at a pressure one to two orders of magnitude lower than experienced in a conventional rocket motor.

Verification of the assumptions made in the analysis must be done experimentally. This could be accomplished by testing the pure end burning configuration in a centerbody type of wind tunnel. The results of the experiments could point the way for further analysis and experimentation.

REFERENCES

1. Billig, F.S. "External Burning in Supersonic Streams." The Johns Hopkins University, Applied Physics Laboratory, TG-912 (AD655460), May 1967.

2. Strahle, W. C. "Theoretical Considerations of Combustion Effects on Base Pressure in Supersonic Flight." Twelfth Symposium (International) on Combustion. 1969, pp 1163-1173.

3. Davis, L. R. "The Effect of Chemical Reactions in the Turbulent Mixing Component on the Dynamics and Thermodynamics of Wake Flow Fields." Ph.D. Thesis, University of Illinois, 1964.

4. Koh, B. L. "Supersonic Base Drag in the Presence of Base Burning." Ph.D. Thesis, Kansas State University, 1966.

5. Corner, J. Theory of the Interior Ballistics of Guns. John Wiley and Sons, Inc., New York, 1950.

6. Reid, J. and Hastings, R. C. "The Effect of a Central Jet on the Base Pressure of a Cylindrical Afterbody in a Supersonic Stream." R&M No. 3224 Aeronautical Research Council, London, England, 1961.

7. Arens, M. and Spiegler, E. "Shock-Induced Boundary Layer Separation in Overexpanded Conical Exhaust Nozzles." AIAA Journal, Vol. 1, No. 3, March 1963, pp 578-581.

8. Sedney, R. "Review of Base Drag." BRL-R-1337 (AD808767), Ballistic Research Laboratories, Aberdeen Proving Ground, Maryland, October 1966.

9. Cole, J. D. and Aroesty, J. "The Blowhard Problem - Inviscid Flows with Surface Injection." Rand Corporation, Santa Monica, California, RM-5196-ARPA, April 1967.

10. Love, E. S., Grigsby, C. E., Lee, L. P., and Woodling, M. J. "Experimental and Theoretical Studies of Axisymmetric Free Jets." NASA TR R-6, 1959.

11. Shapiro, A. H. The Dynamics and Thermodynamics of Compressible Fluid Flow, Vol. 1. The Ronald Press Company, New York, 1953, p 208.

12. Williams, F. A. Combustion Theory. Addison-Wesley Publishing Company, Inc., Reading, Mass. 1965, p 210.

13. Bauer, R. C. "An Analysis of Two-Dimensional Laminar and Turbulent Compressible Mixing." AIAA Journal, Vol. 4, No. 3, 1965, pp 392-395.

14. Fernandez, F. L. Zukoski, E. E. "Supersonic Turbulent Flow with Large Injection." AIAA Journal Vol. 7, No. 9, September 1969, pp 1759-1767.

APPENDIX
ILLUSTRATIONS

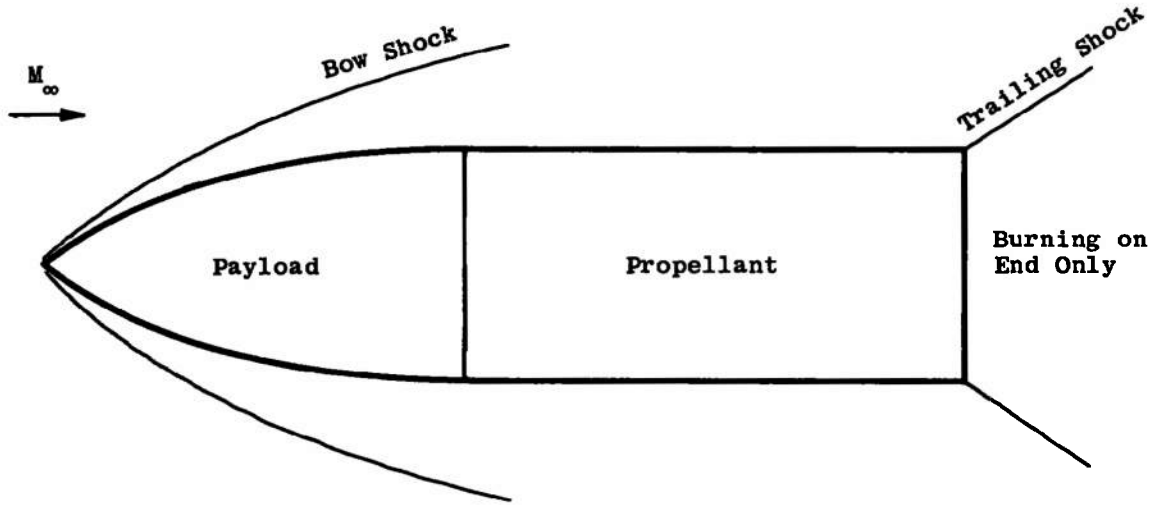

a. Pure End Burning

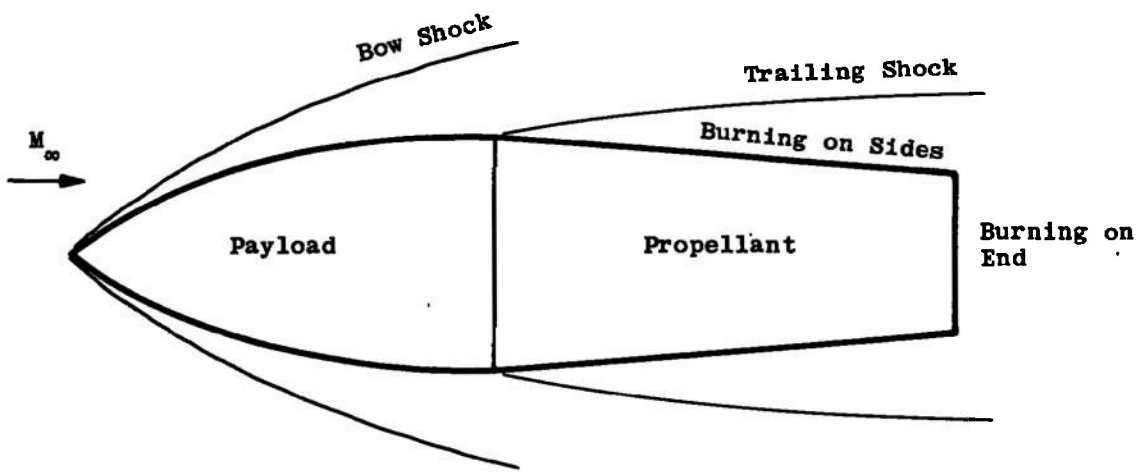

b. Boattail

Fig. 1 Configuration of the Caseless Rocket Motor

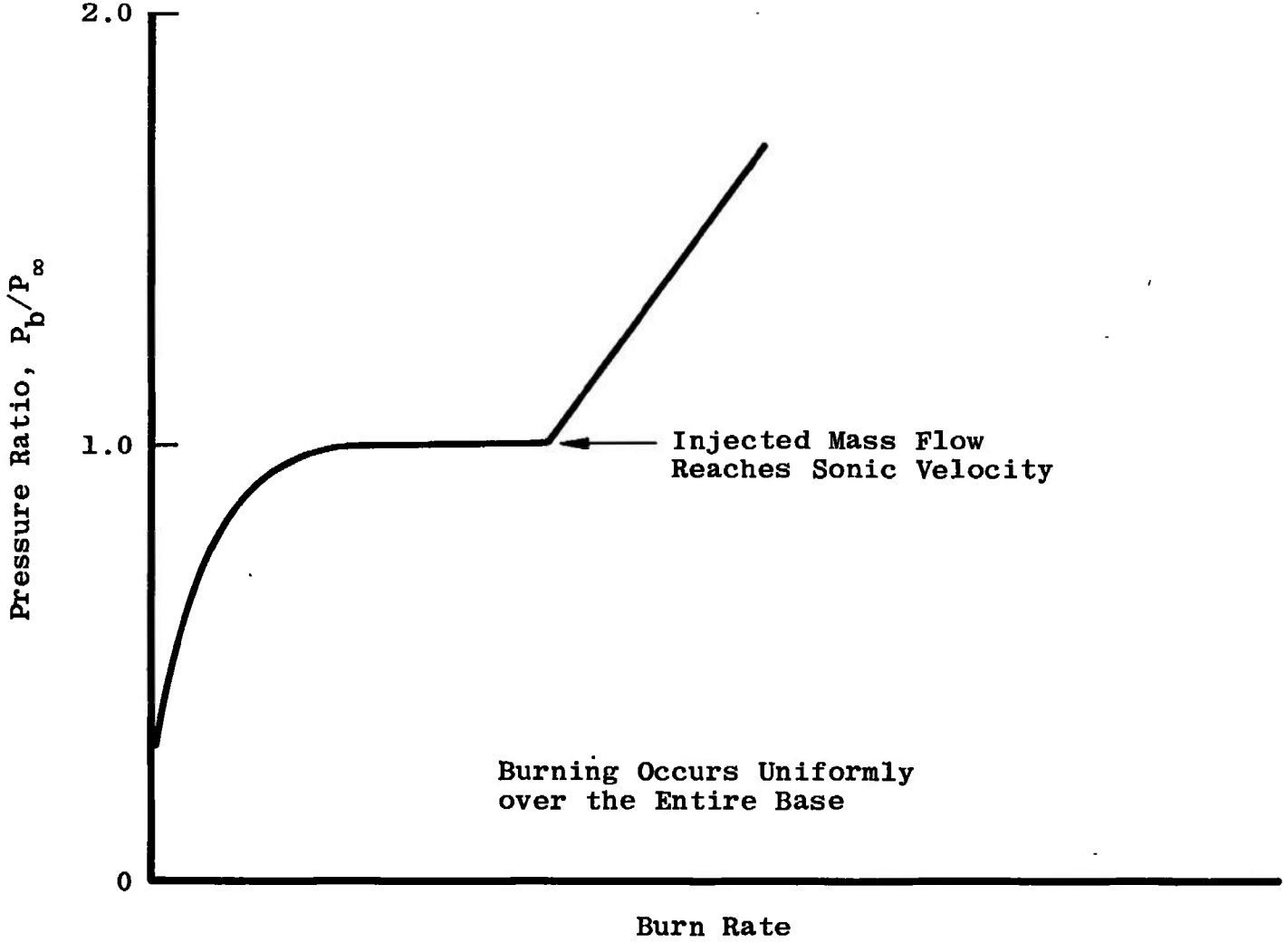

Fig. 2 Base Pressure Ratio versus Dimensionless Burn Rate

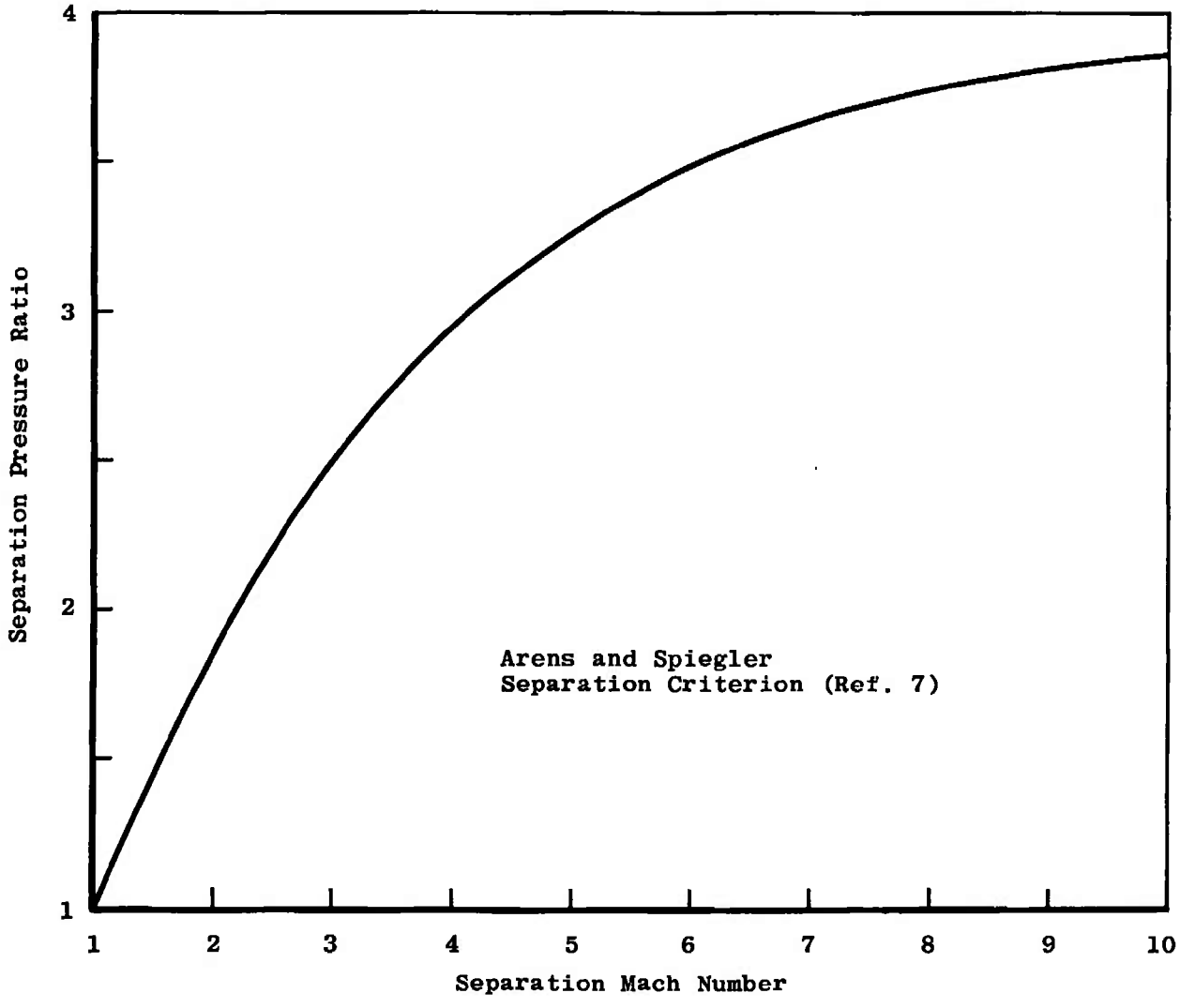

Fig. 3 Boundary Layer Separation Criterion of Arens and Spiegler

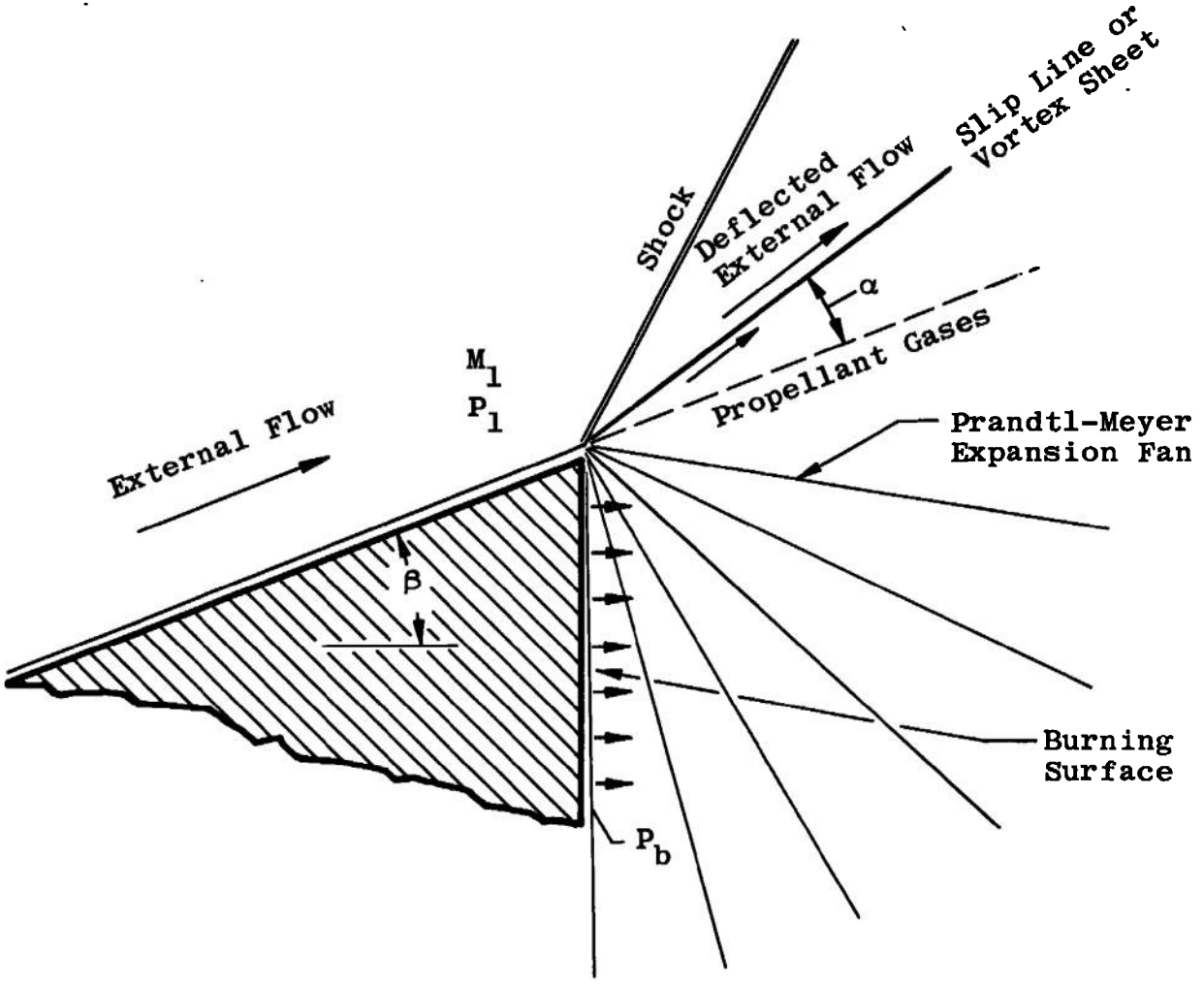

Fig. 4 Schematic of Interaction of External Flow and Propellant Gases

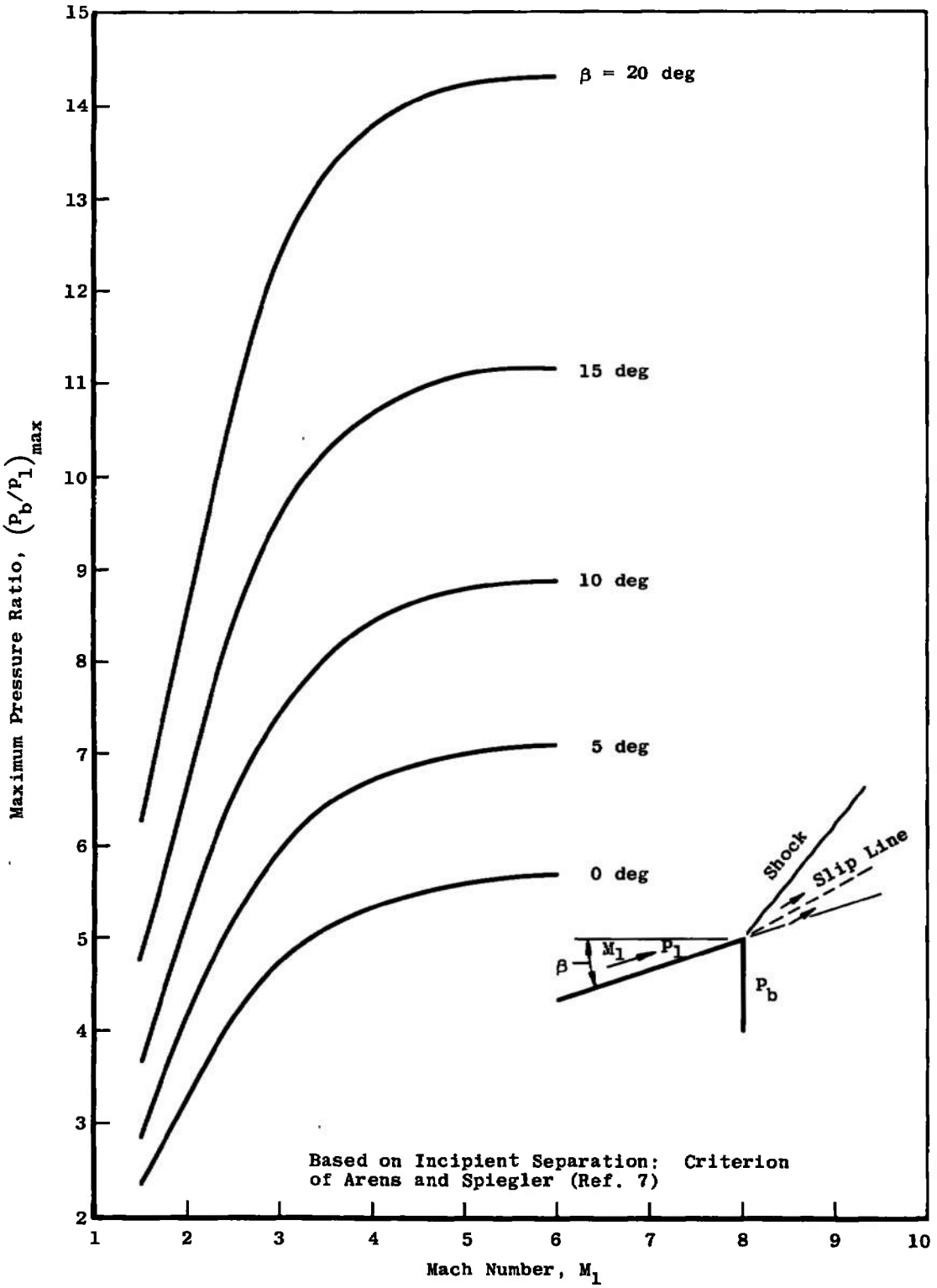

Fig. 5 Maximum Base Pressure

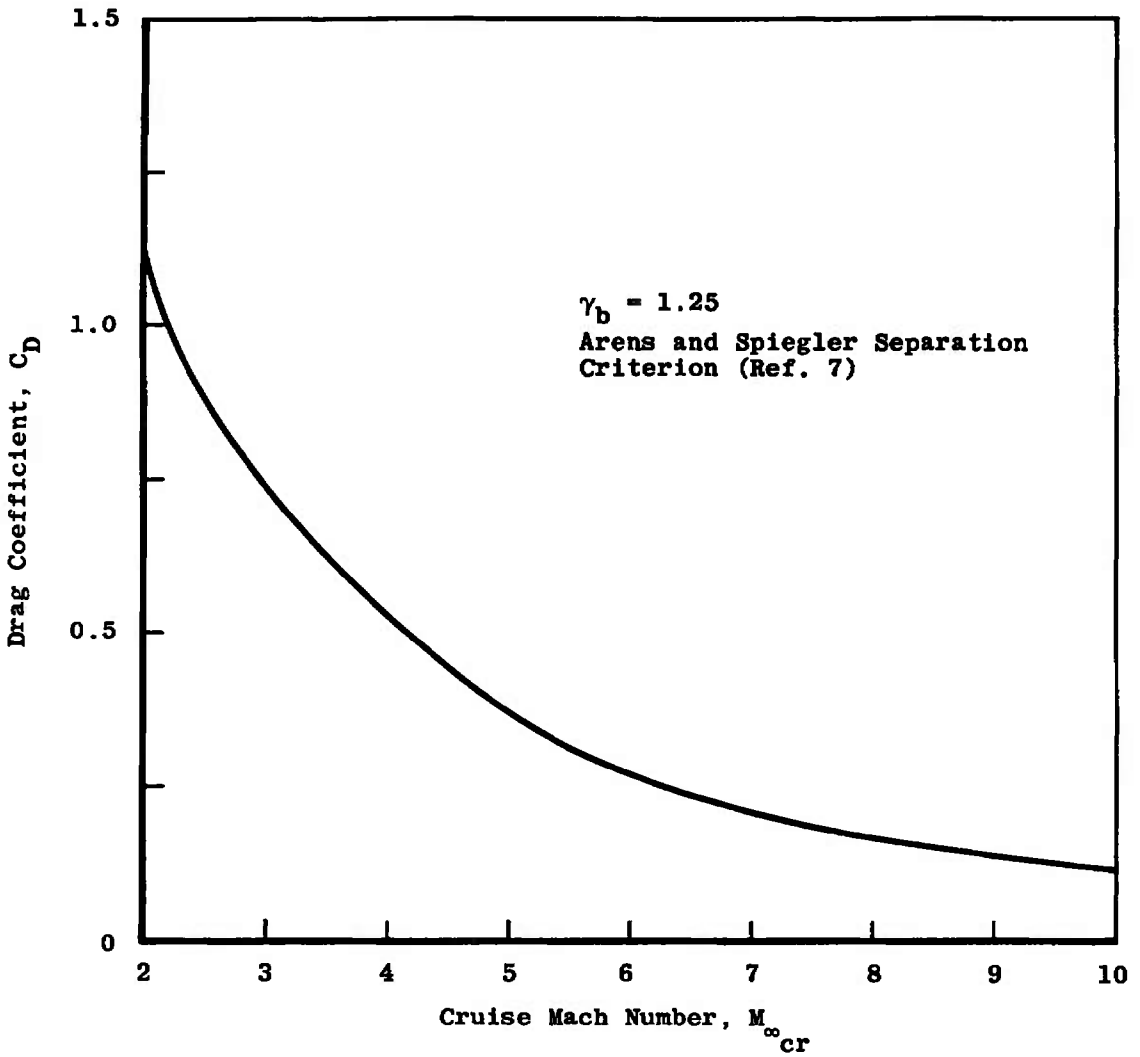

Fig. 6 Forebody Drag Coefficient versus Maximum Cruise Mach Number

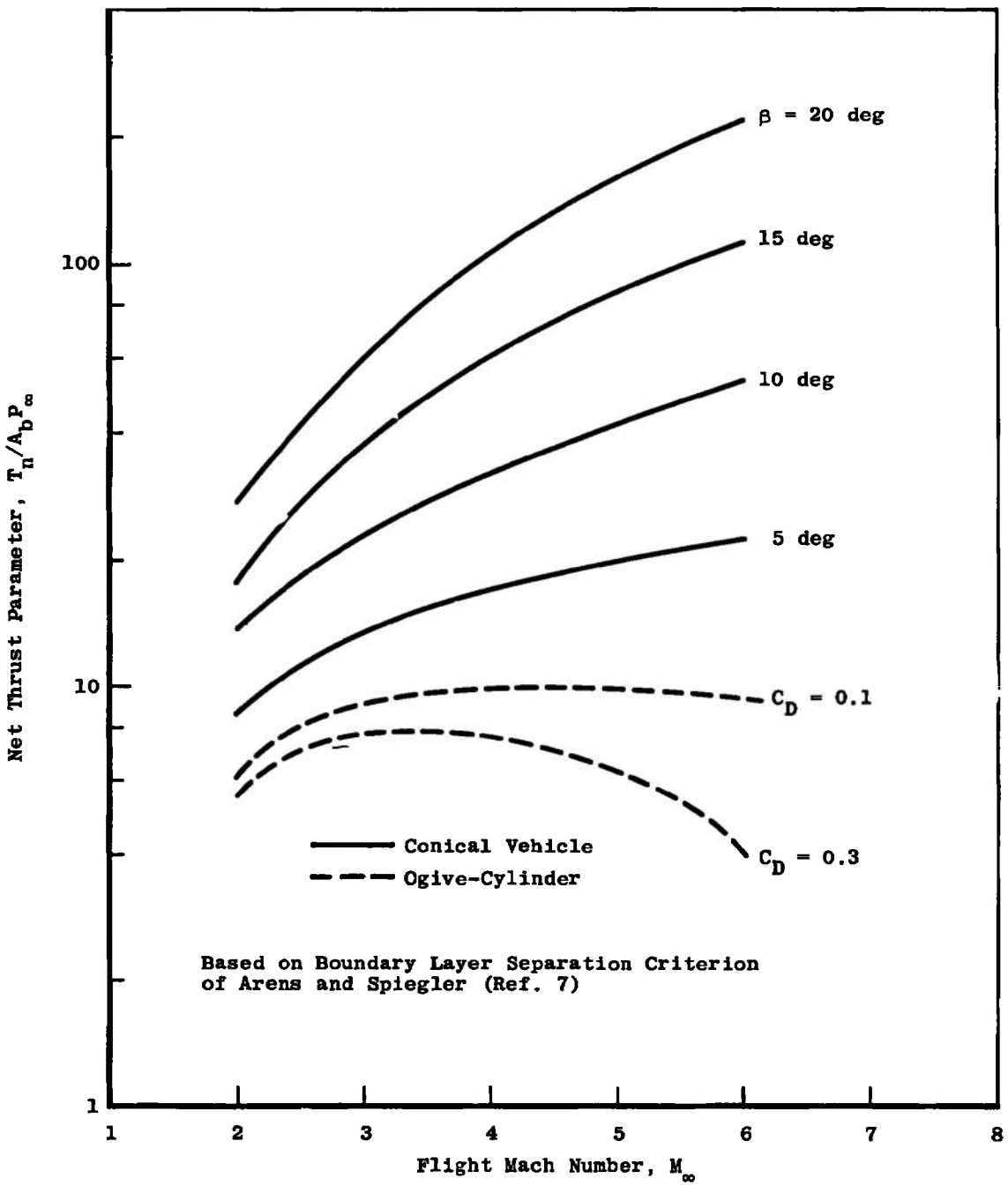

Fig. 7 Maximum Net Thrust Parameter versus Flight Mach Number

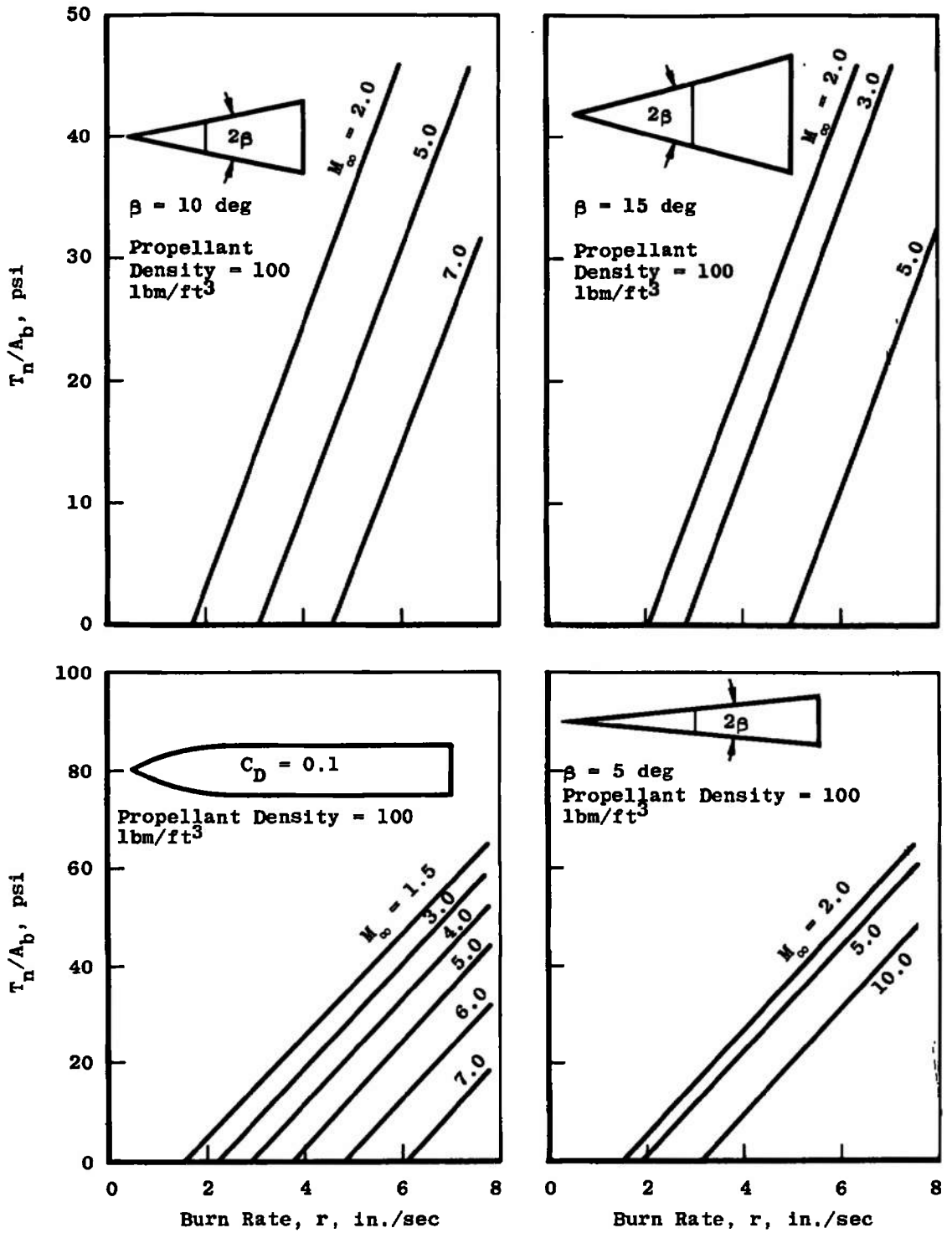

Fig. 8 Net Thrust versus Burn Rate

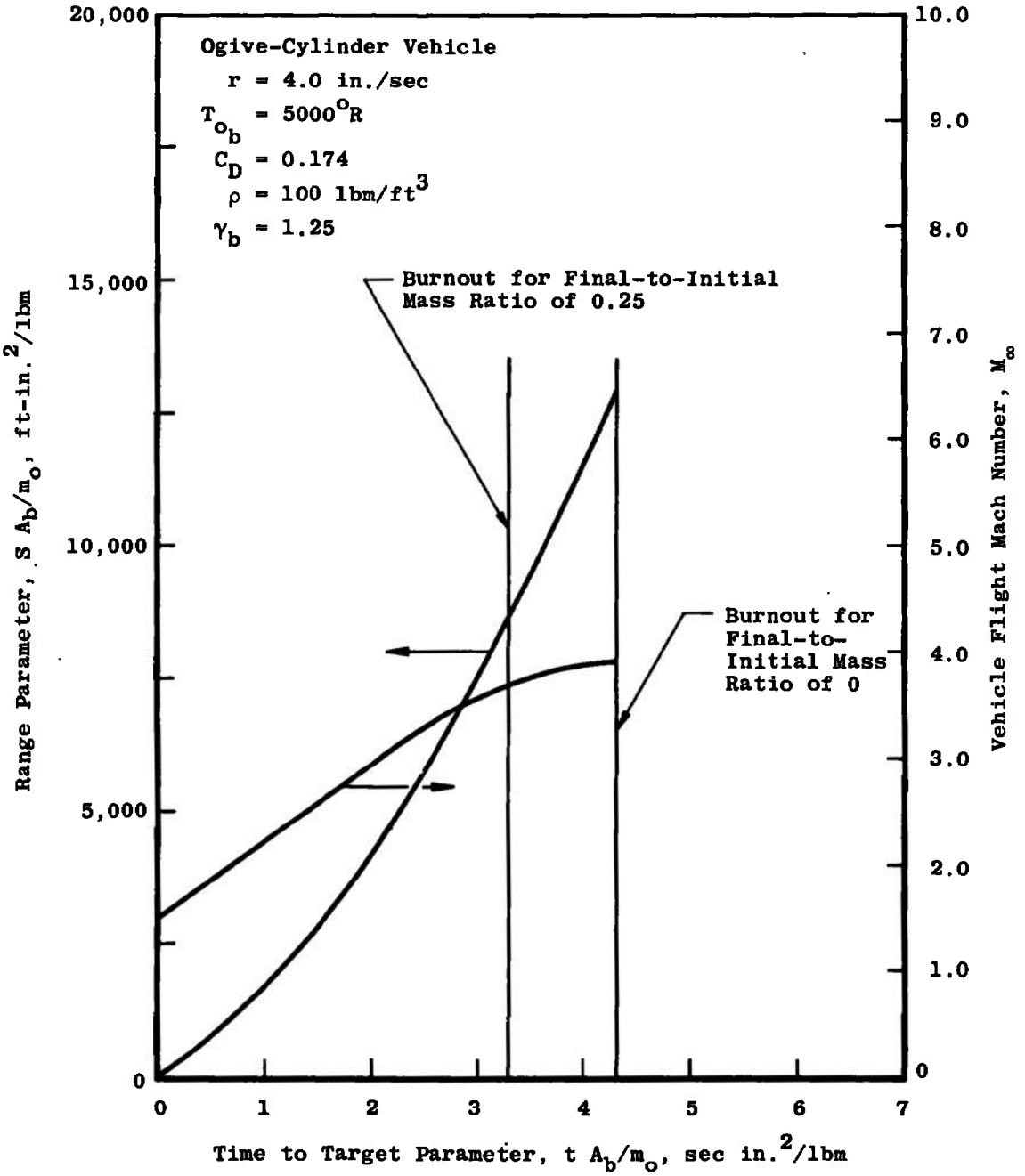

Fig. 9 Range versus Time

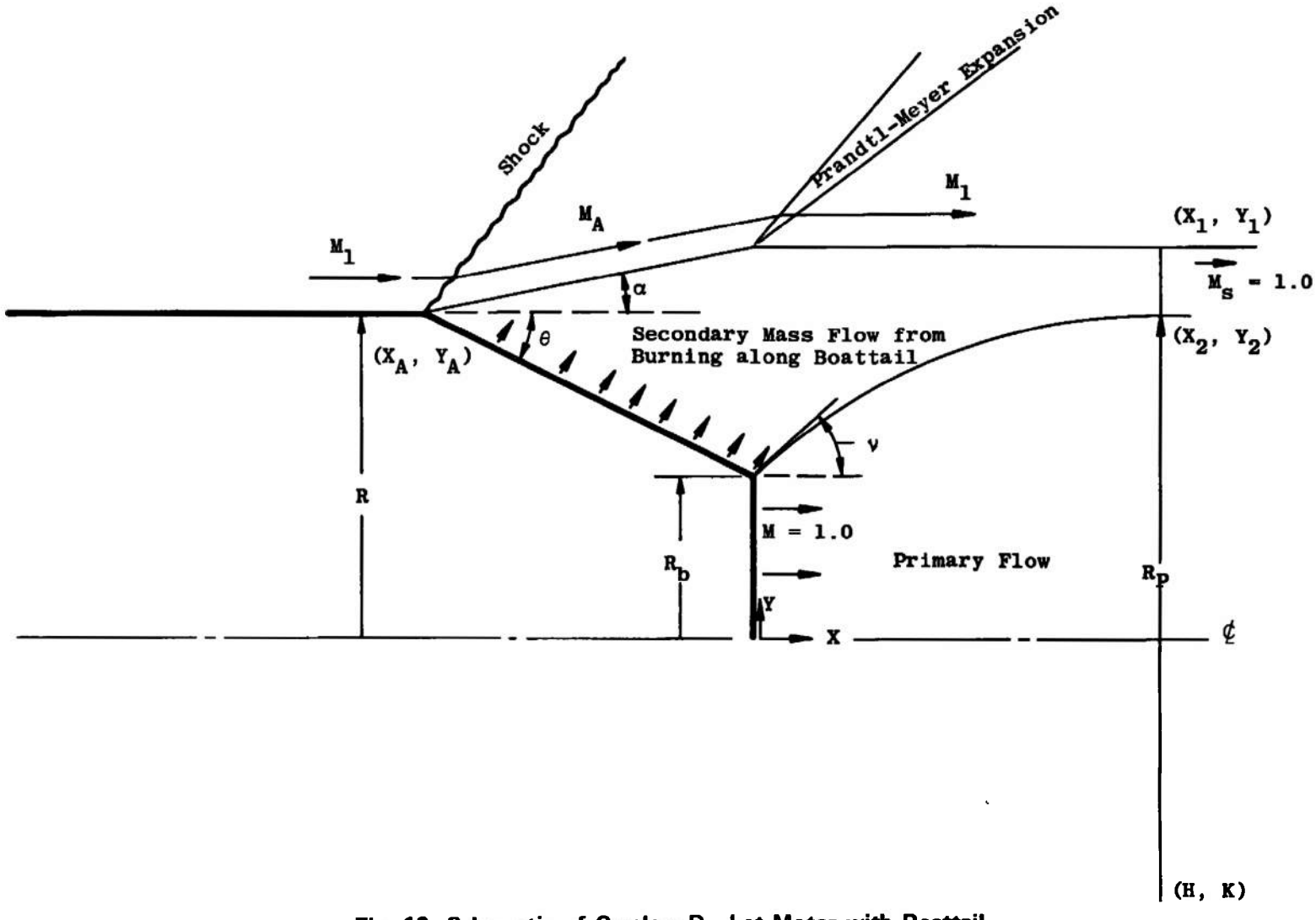

Fig. 10 Schematic of Caseless Rocket Motor with Boattail

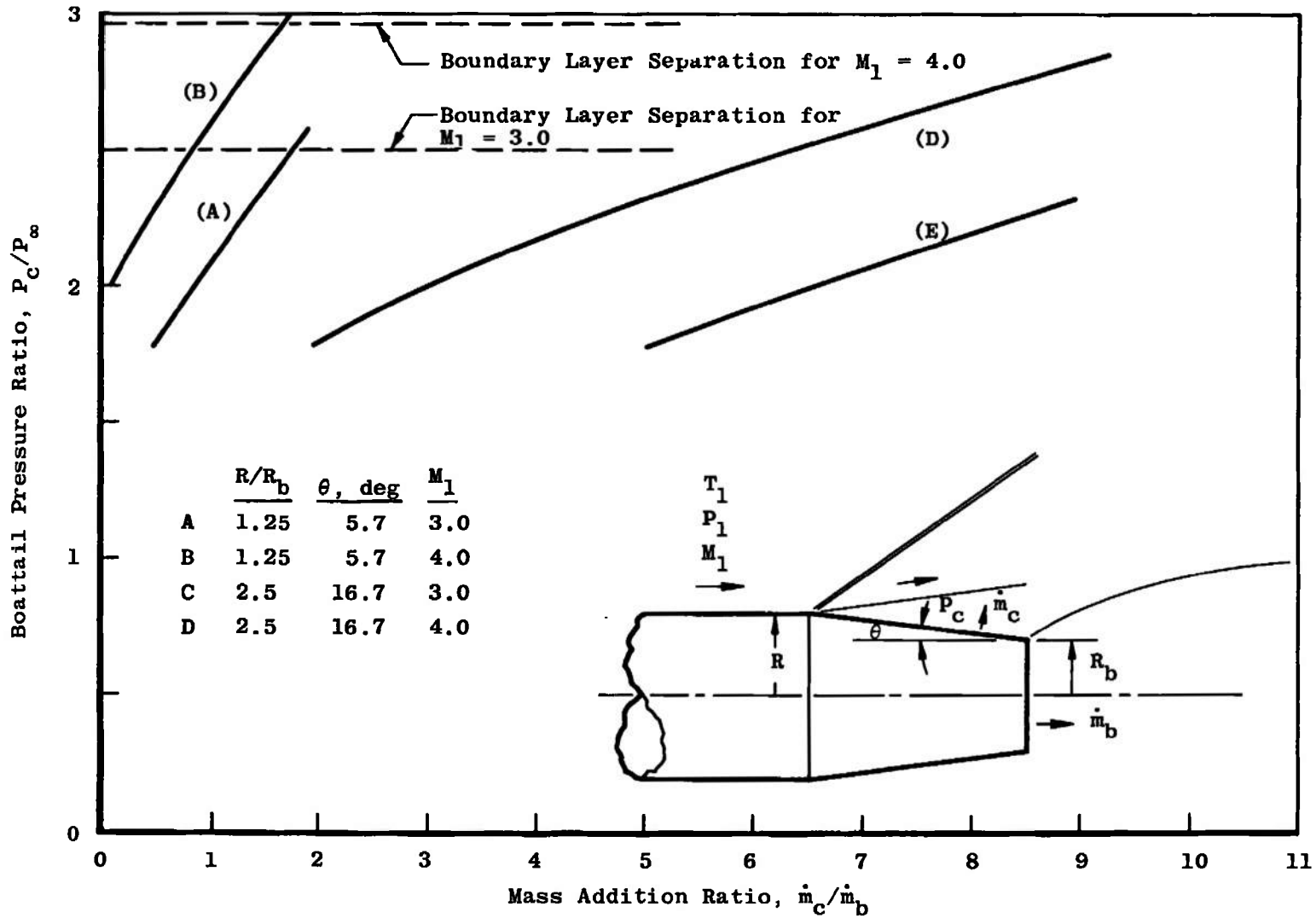

Fig. 11 Boattail Pressure versus Mass Addition Rate along the Boattail

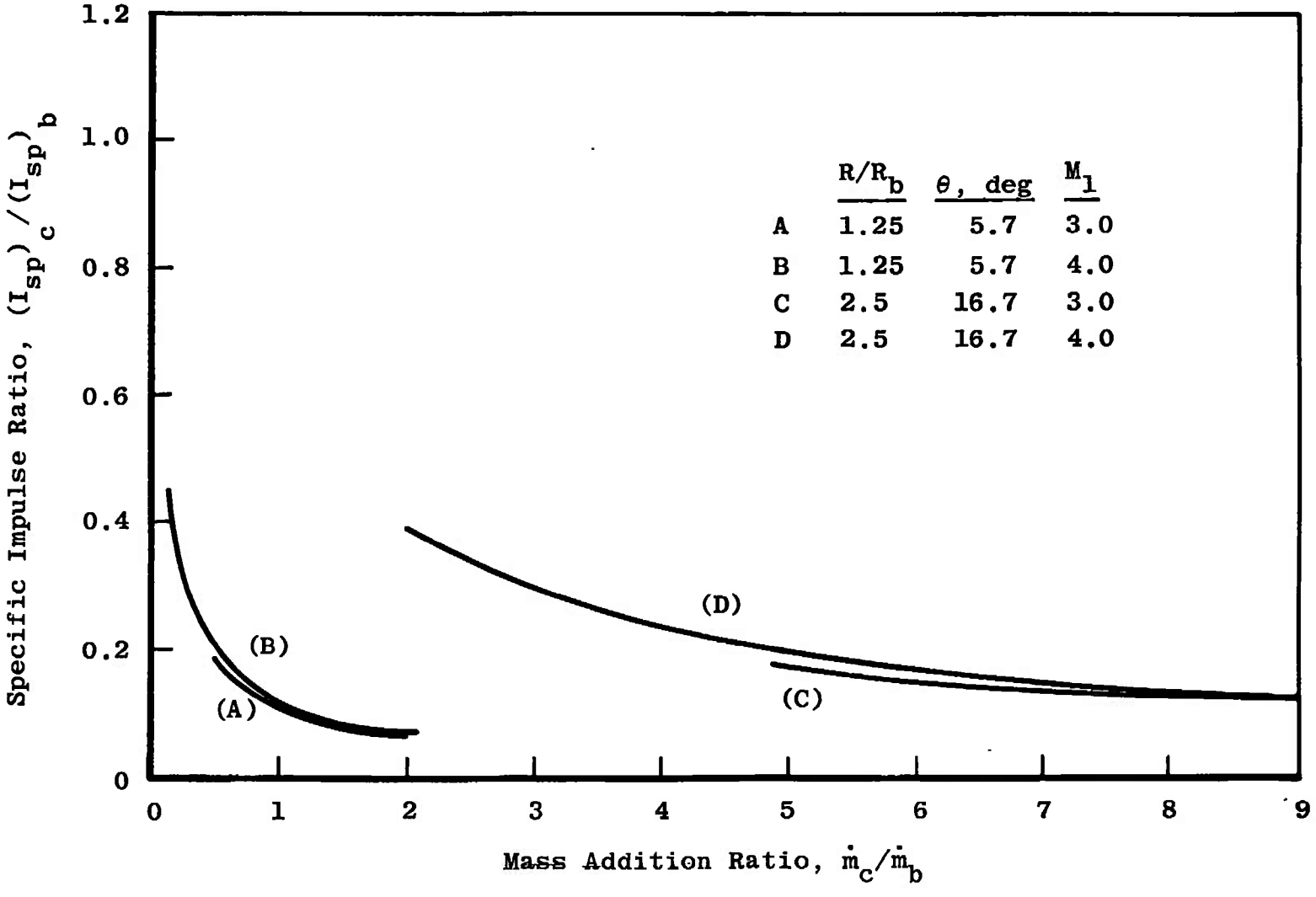

Fig. 12 Specific Impulse of Mass Flow Injected along Boattail versus Boattail Mass Addition Rate

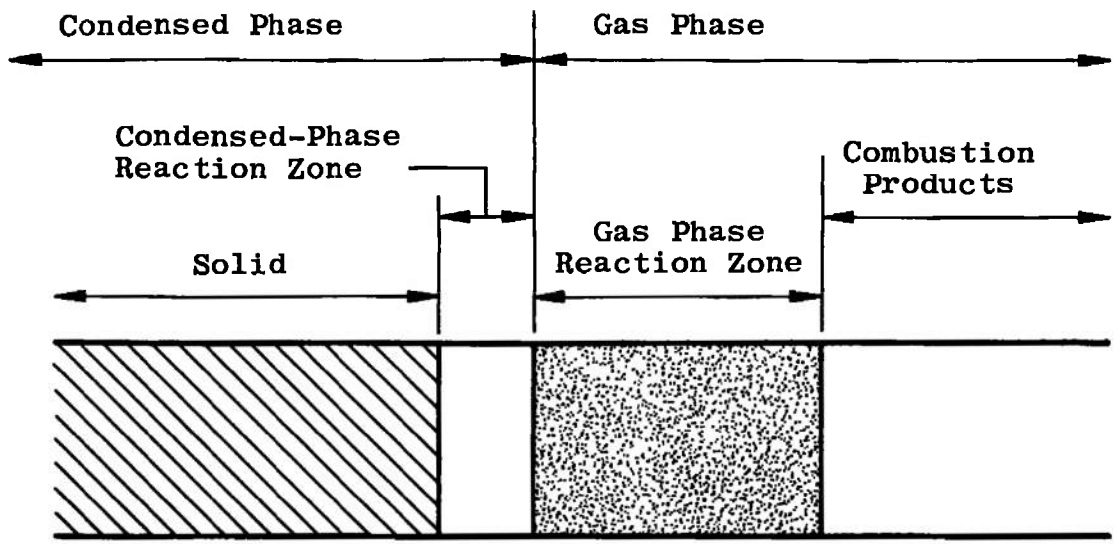

Fig. 13 Schematic of Deflagration in a Solid Propellant

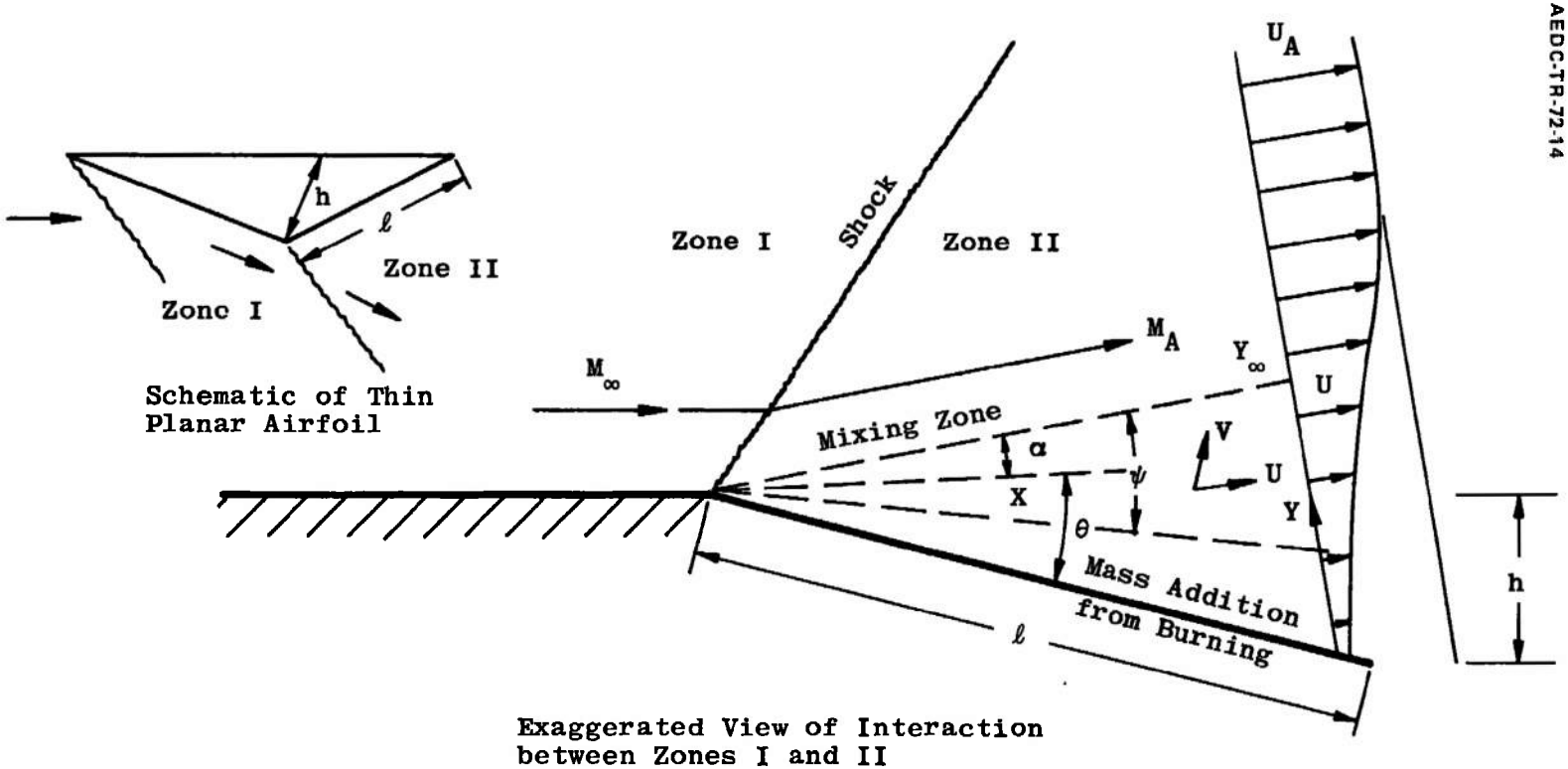

Fig. 14 External Burning Applied to Thin Planar Airfoil for Propulsion or Lift

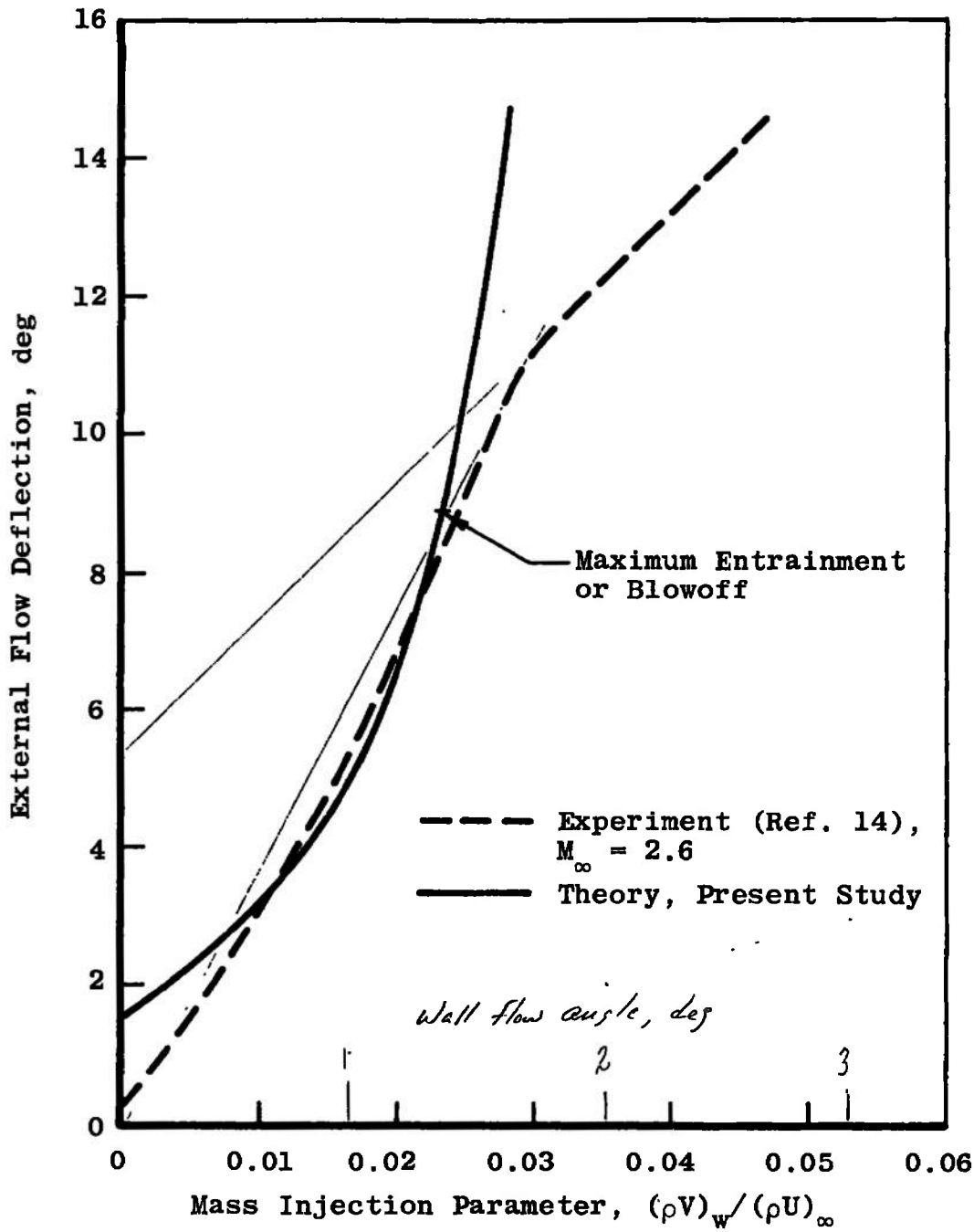

Fig. 15 Comparison of Theory with Experimental Data of Fernandez and Zukoski

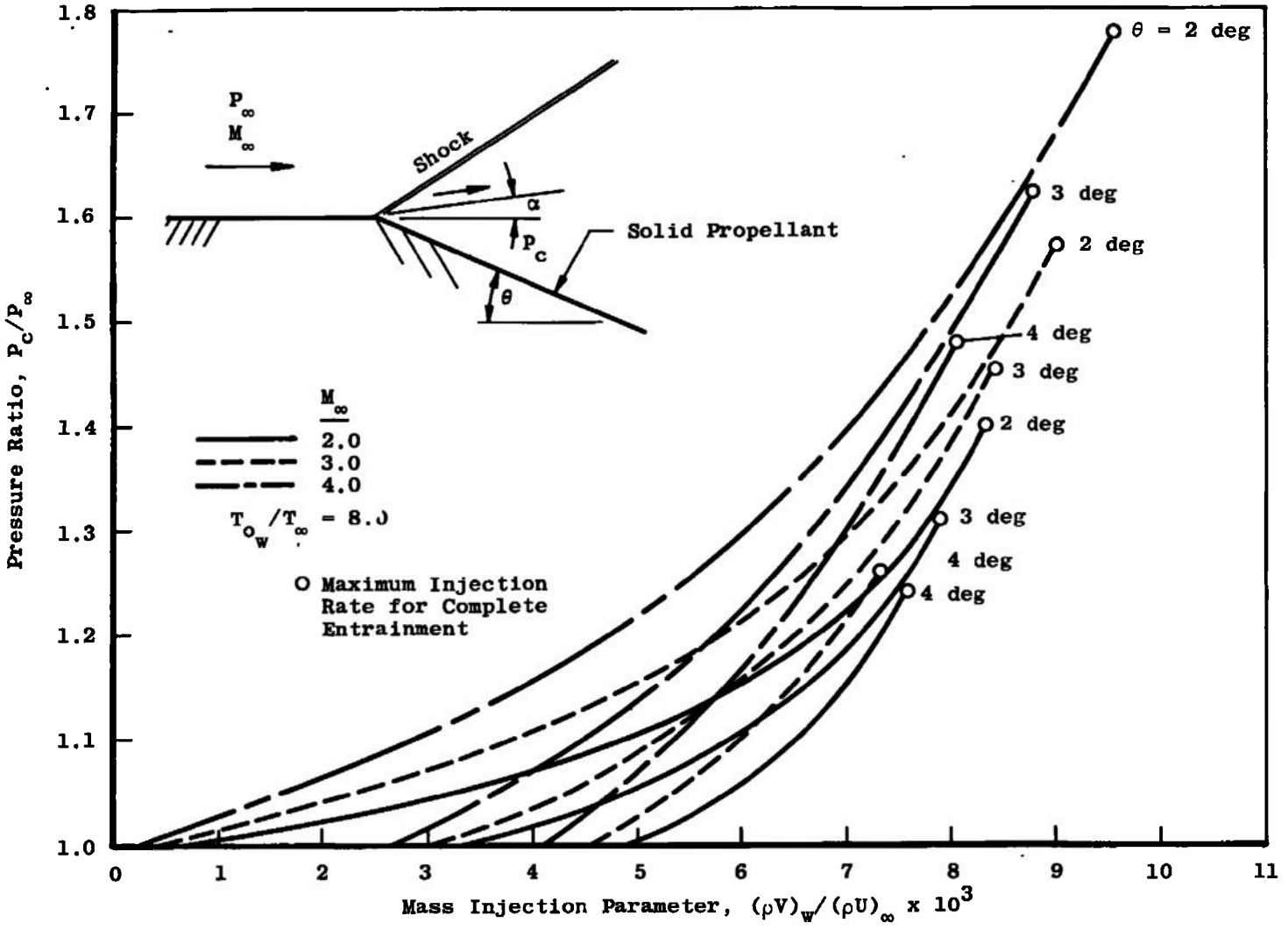

Fig. 16 Pressure Ratio versus Mass Injection Parameter

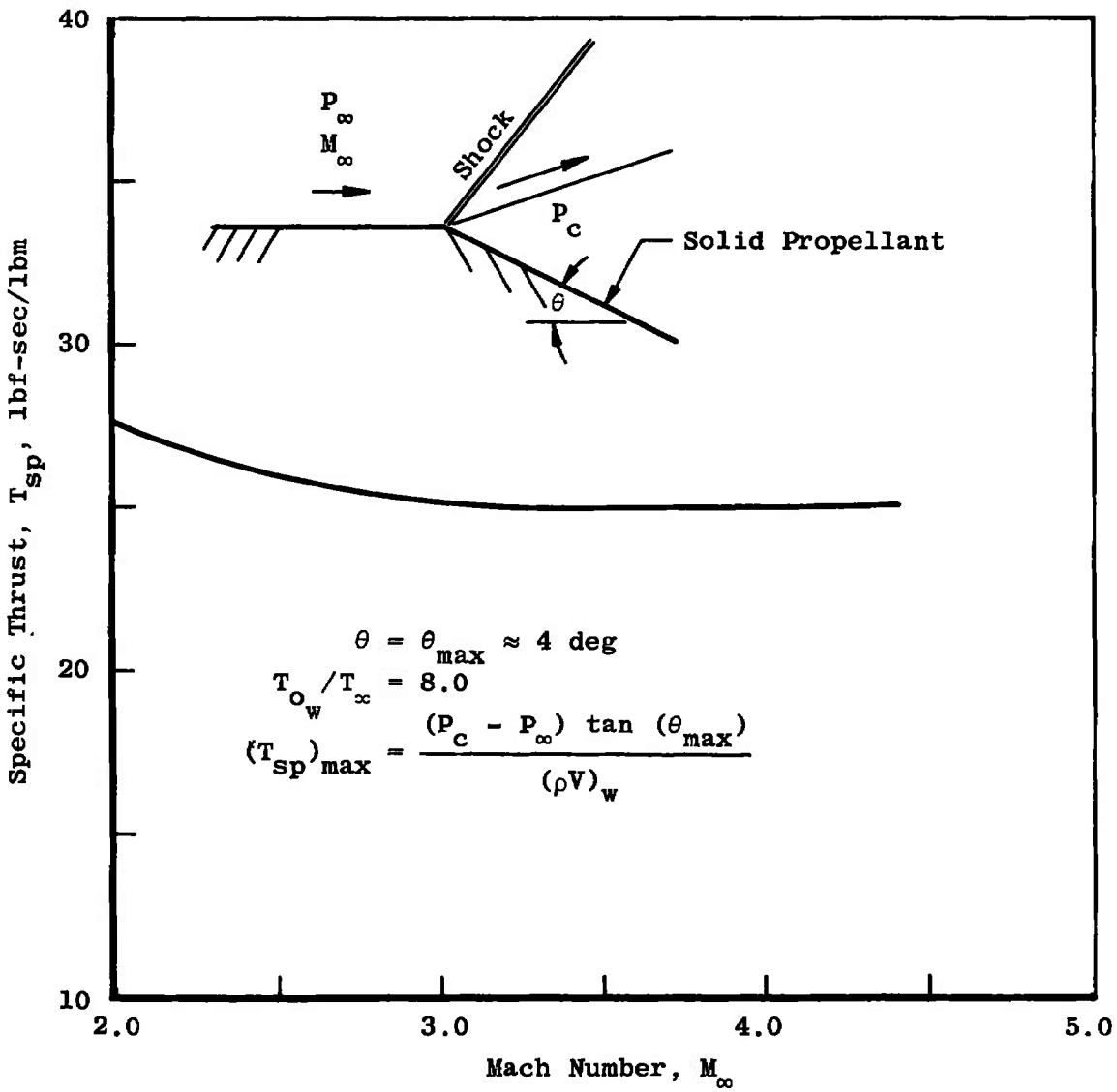

Fig. 17 Specific Thrust for $\theta = \theta_{max}$

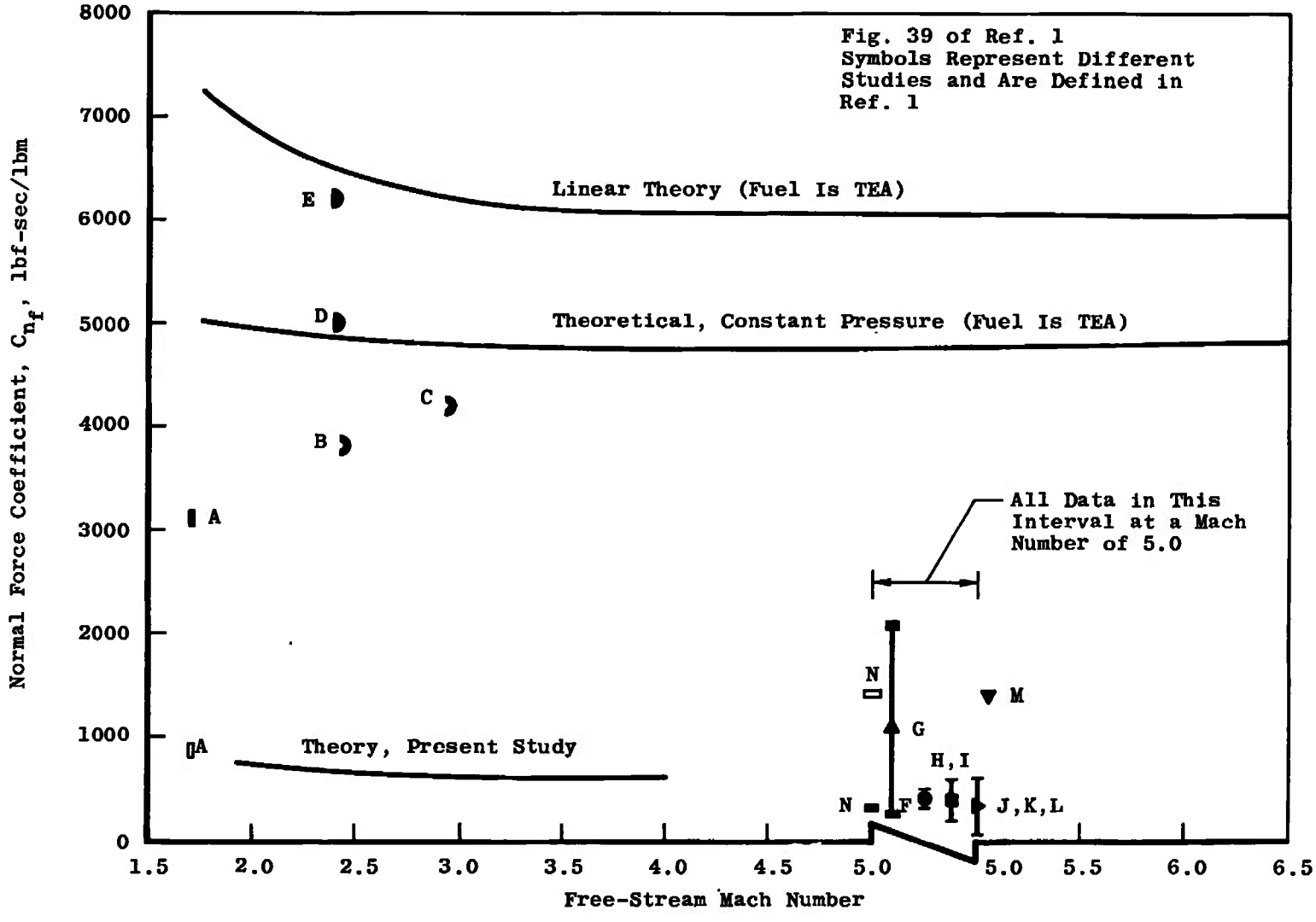

Fig. 18 Normal Force Coefficient as Compiled in Ref. 1

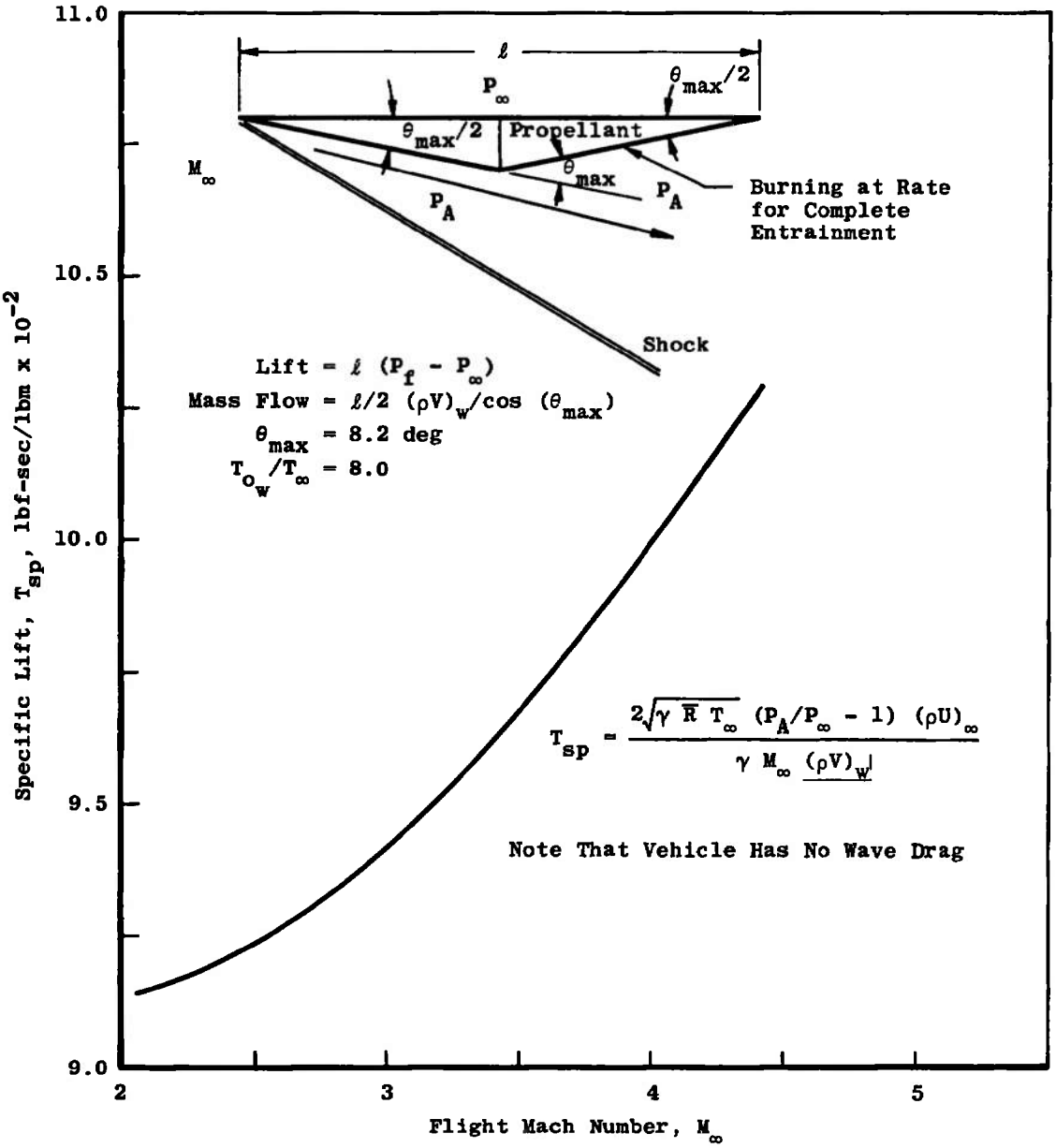

Fig. 19 Specific Lift for Thin Planar Airfoil

UNCLASSIFIED

Security Classification

DOCUMENT CONTROL DATA - R & D

(Security classification of title, body of abstract and indexing annotation must be entered when the overall report is classified)

1. ORIGINATING ACTIVITY (Corporate author)	2a. REPORT SECURITY CLASSIFICATION
Arnold Engineering Development Center, Arnold Air Force Station, Tennessee 37389	UNCLASSIFIED
	2b. GROUP N/A

3 REPORT TITLE

AN ANALYTICAL INVESTIGATION OF THE CASELESS ROCKET MOTOR

4 DESCRIPTIVE NOTES (Type of report and inclusive dates)

June 1970 to June 1971--Final Report

5 AUTHOR(S) (First name, middle initial, last name)

C. E. Willbanks, R. C. Bauer, and P. T. Harsha, ARO, Inc.

6 REPORT DATE	7a. TOTAL NO OF PAGES	7b. NO. OF REFS
February 1972	45	14

8a. CONTRACT OR GRANT NO.	9a. ORIGINATOR'S REPORT NUMBER(S)
b. PROJECT NO. 3059	AEDC-TR-72-14
c. Program Element 61101F	9b. OTHER REPORT NO(S) (Any other numbers that may be assigned this report) ARO-ETF-TR-71-197
d.	

10. DISTRIBUTION STATEMENT

Approved for public release; distribution unlimited.

11. SUPPLEMENTARY NOTES	12. SPONSORING MILITARY ACTIVITY
Available in DDC	Arnold Engineering Development Center (XON), Air Force Systems Command, Arnold AF Station, Tenn.

13 ABSTRACT

An analysis of a caseless and nozzleless solid-propellant rocket motor employing the external burning concept was made. Performance was calculated for a wide range of supersonic flight conditions. The results of the analysis show that acceptable values of specific impulse and thrust are possible for propellants having sufficiently high burn rates in a base burning configuration. The effect of boattailing with combustion along the boattail was investigated and found to degrade the performance. An analysis of a thin planar airfoil with external burning occurring on part of its surface was also made. The specific lift, that is the ratio of the lifting force to propellant flow rate, was found to be an order of magnitude lower than the corresponding specific lift for a conventional airfoil propelled by a turbine engine.

DD FORM 1 NOV 65 1473

UNCLASSIFIED

Security Classification

14. KEY WORDS	LINK A		LINK B		LINK C	
	ROLE	WT	ROLE	WT	ROLE	W
M						
mathematical model						
caseless and nozzleless rocket						
solid propellant rocket motor						
external combustion						
performance						
calculations						
mathematical analysis						